Data analysis of gravitational-wave signals from spinning neutron stars. I. The signal and its detection

Piotr Jaranowski[1,3]   Andrzej Królak[1,4]

Bernard F. Schutz[1,2]

[1] *Albert-Einstein-Institut, Max-Planck-Institut für Gravitationsphysik*

Schlaatzweg 1, 14473 Potsdam, Germany

[2] *Department of Physics and Astronomy, University of Wales College of Cardiff*

PO BOX 913, Cardiff, U.K.

[3] *Institute of Physics, Białystok University*

Lipowa 41, 15-424 Białystok, Poland

[4] *Institute of Mathematics, Polish Academy of Sciences*

Śniadeckich 8, 00-950 Warsaw, Poland

February 3, 2008

Abstract

We present a theoretical background for the data analysis of the gravitational-wave signals from spinning neutron stars for Earth-based laser interferometric detectors. We introduce a detailed model of the signal including both the frequency and the amplitude modulations. We include the effects of the intrinsic frequency changes and the modulation of the frequency at the detector due to the Earth motion. We estimate the effects of the star's proper motion and of relativistic corrections. Moreover we consider a signal consisting of two components corresponding to a frequency f and twice that frequency. From the maximum likelihood principle we derive the detection statistics for the signal and we calculate the probability density function of the statistics. We obtain the data analysis procedure to detect the signal and to estimate its parameters. We show that for optimal detection of the amplitude modulated signal we need four linear filters instead of one linear filter needed for a constant amplitude signal. Searching for the doubled frequency signal increases further the number of linear filters by a factor of two. We indicate how the fast Fourier transform algorithm and resampling methods commonly proposed in the analysis of periodic signals can be used to calculate the detection statistics for our signal. We find that the probability density function of the detection statistics is determined by one parameter: the optimal signal-to-noise ratio. We study the signal-to-noise ratio by means of the Monte Carlo method for all long-arm interferometers that are currently under construction. We show how our analysis can be extended to perform a joint search for periodic signals by a network of detectors and we perform Monte Carlo study of the signal-to-noise ratio for a network of detectors.

1 Introduction

Spinning neutron stars are one of the primary candidate sources of gravitational waves for long-arm laser interferometric detectors ([1], see [2] for a review). Detectors with a sufficent sensitivity to see strong neutron star sources anywhere in the Galaxy will be taking data within two or three years [3, 4, 5, 6]. A rotating body, perfectly symmetric about its rotation axis does not emit gravitational waves. If the spinning neutron star is to emit gravitational waves over extended periods of time, it must have some kind of long-lived asymmetry. Several mechanisms have been given for such an asymmetry to arise [7, 8, 9, 10]. During the crystalization period the crust of the neutron star may develop deviations from axisymmetry that will be supported by anisotropic stresses in the solid crust [7]. The strong magnetic field present in the neutron star may not be aligned with the rotation axis and consequently the distortion produced by the magnetic pressure results in the neutron star being asymmetric [8]. Also the rotation axis may not coincide with a principal axis of the star's moment of inertia tensor. Then the star will precess and

emit gravitational waves [9, 10]. There are other mechanisms that can produce gravitational waves from neutron stars. Accretion of matter on a neutron star can drive it into a nonaxisymmetric configuration and power steady radiation with a considerable amplitude. This mechanism has been pointed out by Wagoner ([11], see also [12]). It applies to a certain class of neutron stars, including accreting stars in binary systems that have been spun up to the first instability point of the Chandrasekhar-Friedman-Schutz (CFS) instability [13, 14]. Recently Andersson [16] suggested a similar instability in $r-$modes of rotating relativistic stars. The effectiveness of these instabilities depends on the viscocity of the star which in turn is determined by the temperature of the star [17].

This paper initiates a series of papers where theoretical problems of data analysis of gravitational-wave signals from spinning neutron stars are considered, independently of the mechanisms generating the waves.

The data analysis of monochromatic signals for interferometric antennae was investigated by one of us [15]. A search strategy for such signals was proposed and the computing power required estimated. The basic method to detect periodic signals is to Fourier analyse the data, and an efficient computational tool is the fast Fourier transform. The main problem is that to do the search one has to take into account the modulation of the signal due to the Earth's motion relative to the solar system barycenter. If the position of the source on the sky is unknown this introduces two additional parameters in the signal and this vastly increases the computational time to do the search. It is clear that the main limit on the sensitivity of such a search will be the available computing power. Variants of the proposed search strategy have been implemented with test data from the prototype detectors where the search was carried out only over a limited region of the parameter space [18, 19, 20].

The problem of computational requirements has recently been reconsidered by Brady et al. [21]. They realized that in the model of the signal the effect of the intrinsic frequency modulation due to spin-down or spin-up of the neutron star needs to be considered. This increases the parameter space and consequently the computational power required to search all the parameter space. Assuming access to teraflops computing power it was shown that coherent integration times will be limited to days for an all-sky search for young, rapidly spinning stars and to weeks for more directed searches. A simplified model of the signal where modulation due to diurnal rotation of the Earth was neglected has also been examined by one of us [22] and the computational requirements to do the search were estimated.

In this series of papers we consider a more general model of the signal than in the work cited above. We take into account not only the modulation of the phase of the signal but also the amplitude modulation. Moreover we consider a signal consisting of two components corresponding to a frequency f and twice that frequency. In general neither of the components is dominant.

In this work, which is Paper I of the series, we introduce the signal and we derive an optimal data analysis procedure for its detection. In Paper II we examine the accuracy of estimation of the parameters of the signal that can be achieved with the optimal analysis. In Paper III we examine in detail the characteristics of the detection statistics derived in Paper I and the computational power required to calculate it. In Paper IV we investigate the least-squares method to estimate astrophysically interesting parameters of the signal from the estimators of the amplitudes derived in Paper I.

The plan of this paper is as follows. In Section 2 we derive a general formula for the response of a laser interferometer to our two component signal including both the phase and the amplitude modulation. In Section 3 from the maximum likelihood principle we derive the data analysis procedure to detect the signal introduced in Section 2 and to estimate its parameters. We obtain the basic probability density functions of the detection statistics. We show that probability of detection is determined by one parameter: the optimal signal-to-noise ratio. We study this quantity by means of the Monte Carlo simulations for all the interferometric detectors that are currently under construction. We conclude Section 3 by showing how one can take advantage of the speed of the FFT algorithm to evaluate efficiently our detection statistics. This involves application of the resampling techniques proposed earlier for the case of a simpler signal model [15, 21]. In Section 4 we show that our analysis can easily be extended to networks of detectors and we perform a Monte Carlo study of the signal-to-noise ratio for the networks. In Appendix A we discuss the model of the phase of the gravitational-wave signal and in particular we estimate the effect of the proper motion of the neutron star and of relativistic corrections. In Appendix B we give the general analytic formula for the optimal signal-to-noise ratio. In Appendix C we present an additional study by means of the Monte Carlo simulations of the signal-to-noise ratios for the individual components of the spinning neutron star signal.

2 Noise-free response of the interferometric detector

2.1 Beam-pattern functions

The response of a laser interferometric detector to a weak plane gravitational wave in the long wavelength approximation (i.e. when the size of the detector is much smaller than the reduced wavelength $\lambda/(2\pi)$ of the wave) is well known (see, e.g., [23] and Section IIA of [24] and references therein). The dimensionless detector's response function h is defined as the difference between the wave induced relative length changes of the two interferometer arms and can be computed from the formula (cf. Eq. (5) of [24])

$$h(t) = \frac{1}{2}\mathbf{n}_1 \cdot \left[\widetilde{H}(t)\mathbf{n}_1\right] - \frac{1}{2}\mathbf{n}_2 \cdot \left[\widetilde{H}(t)\mathbf{n}_2\right], \tag{1}$$

where $\mathbf{n}_1$ and $\mathbf{n}_2$ denote the unit vectors parallel to the arm number 1 and 2, respectively (the order of arms if defined such that the vector $\mathbf{n}_1 \times \mathbf{n}_2$ points *outwards* from the surface of the Earth), $\widetilde{H}$ is the 3-dimensional matrix of the spatial metric perturbation produced by the wave in the proper reference frame of the detector, and a dot stands for the standard scalar product in the 3-dimensional Cartesian space. The matrix $\widetilde{H}$ is given by

$$\widetilde{H}(t) = M(t)H(t)M(t)^T, \tag{2}$$

where M is the 3-dimensional orthogonal matrix of transformation from the wave Cartesian coordinates (x_w, y_w, z_w) to the Cartesian coordinates $(x_{\mathrm{d}}, y_{\mathrm{d}}, z_{\mathrm{d}})$ in the detector's proper reference frame (the definition of these coordinates is given below), T denotes matrix transposition. In the wave coordinate system the gravitational wave travels in the $+z_w$ direction. In this frame the matrix H has the form

$$H(t) = \begin{pmatrix} h_+(t) & h_\times(t) & 0 \\ h_\times(t) & -h_+(t) & 0 \\ 0 & 0 & 0 \end{pmatrix}, \tag{3}$$

where the functions h_+ and $h_\times$ describe two independent wave's polarizations. Collecting Eqs. (1)–(3) together one can see that the response function h is a linear combination of the functions h_+ and $h_\times$:

$$h(t) = F_+(t)h_+(t) + F_\times(t)h_\times(t), \tag{4}$$

where F_+ and $F_\times$ are called the *beam-pattern* functions.

   Because of the diurnal motion of the Earth the beam-patterns F_+ and $F_\times$ are periodic functions of time with a period equal to one sidereal day. We want now to extract explicitly this time dependence as well as to express F_+ and $F_\times$ as functions of right ascension α and declination δ of the gravitational-wave source and polarization angle ψ (the angles α, δ, and ψ determine the orientation of the wave reference frame with respect to the celestial sphere reference frame defined below). Our treatment partially follows that of Section 5 of [8]. We represent the matrix M of Eq. (2) as

$$M = M_3 M_2 M_1^T, \tag{5}$$

where M_1 is the matrix of transformation from wave to celestial sphere frame coordinates, M_2 is the matrix of transformation from celestial coordinates to cardinal coordinates and M_3 is the matrix of transformation from cardinal coordinates to detector proper reference frame coordinates. In celestial sphere coordinates the z axis coincides with the Earth's rotation axis and points toward the North pole, the x and y axes lie in the Earth's equatorial plane, and the x axis points toward the vernal point. In cardinal coordinates the (x, y) plane is tangent to the surface of the Earth at detector's location with x axis in the North-South direction and y axis in the West-East direction, the z cardinal axis is along the Earth's radius pointing toward zenith. In detector coordinates the z axis coincides with the z axis of cardinal coordinates and the x axis is along the first interferometer arm (then the y axis is along the second arm if the arms are at a right angle). Under the above conventions the matrices M_1, M_2, and M_3 are as follows (matrices M_1 and M_2 given below coincide with matrices A and B from Ref. [8], cf. Eqs. (52) and (60) of [8])

$$M_1 = \begin{pmatrix} \sin\alpha\cos\psi - \cos\alpha\sin\delta\sin\psi & -\cos\alpha\cos\psi - \sin\alpha\sin\delta\sin\psi & \cos\delta\sin\psi \\ -\sin\alpha\sin\psi - \cos\alpha\sin\delta\cos\psi & \cos\alpha\sin\psi - \sin\alpha\sin\delta\cos\psi & \cos\delta\cos\psi \\ -\cos\alpha\cos\delta & -\sin\alpha\cos\delta & -\sin\delta \end{pmatrix}, \tag{6}$$

3

$$M_2 = \begin{pmatrix} \sin\lambda\cos(\phi_r + \Omega_r t) & \sin\lambda\sin(\phi_r + \Omega_r t) & -\cos\lambda \\ -\sin(\phi_r + \Omega_r t) & \cos(\phi_r + \Omega_r t) & 0 \\ \cos\lambda\cos(\phi_r + \Omega_r t) & \cos\lambda\sin(\phi_r + \Omega_r t) & \sin\lambda \end{pmatrix}, \tag{7}$$

$$M_3 = \begin{pmatrix} -\sin(\gamma + \zeta/2) & \cos(\gamma + \zeta/2) & 0 \\ -\cos(\gamma + \zeta/2) & -\sin(\gamma + \zeta/2) & 0 \\ 0 & 0 & 1 \end{pmatrix}. \tag{8}$$

In Eq. (7) λ is the latitude of the detector's site, Ω_r is the rotational angular velocity of the Earth, and ϕ_r is a deterministic phase which defines the position of the Earth in its diurnal motion at $t = 0$ (the sum $\phi_r + \Omega_r t$ coincides with the local sidereal time of the detector's site, i.e. with the angle between the local meridian and the vernal point). In Eq. (8) γ determines the orientation of the detector's arms with respect to local geographical directions: γ is measured counter-clockwise from East to the bisector of the interferometer arms, and ζ is the angle between the interferometer arms. The vectors $\mathbf{n}_1$ and $\mathbf{n}_2$ from Eq. (1) in the detector's reference frame have coordinates

$$\mathbf{n}_1 = (1, 0, 0), \quad \mathbf{n}_2 = (\cos\zeta, \sin\zeta, 0). \tag{9}$$

The values of the angles λ, γ, ζ, and the longitudes L (measured positively westwards) for different detectors can be found in Table 1 [25].

detector	λ (degrees)	L (degrees)	γ (degrees)	ζ (degrees)
GEO600	52.25	−9.81	68.775	94.33
LIGO Hanford	46.45	119.41	171.8	90
LIGO Livingston	30.56	90.77	243.0	90
VIRGO	43.63	−10.5	116.5	90
TAMA300	35.68	−139.54	225.0	90

Table 1: Positions and orientations of detectors.

To find the explicit formula for F_+ and $F_\times$ we have to combine Eqs. (1)–(9). After extensive algebraic manipulations we arrive at the expressions:

$$F_+(t) = \sin\zeta\left[a(t)\cos 2\psi + b(t)\sin 2\psi\right], \tag{10}$$
$$F_\times(t) = \sin\zeta\left[b(t)\cos 2\psi - a(t)\sin 2\psi\right], \tag{11}$$

where

$$\begin{aligned} a(t) = \ & \frac{1}{16}\sin 2\gamma(3 - \cos 2\lambda)(3 - \cos 2\delta)\cos[2(\alpha - \phi_r - \Omega_r t)] \\ & -\frac{1}{4}\cos 2\gamma\sin\lambda(3 - \cos 2\delta)\sin[2(\alpha - \phi_r - \Omega_r t)] \\ & +\frac{1}{4}\sin 2\gamma\sin 2\lambda\sin 2\delta\cos[\alpha - \phi_r - \Omega_r t] \\ & -\frac{1}{2}\cos 2\gamma\cos\lambda\sin 2\delta\sin[\alpha - \phi_r - \Omega_r t] \\ & +\frac{3}{4}\sin 2\gamma\cos^2\lambda\cos^2\delta, \end{aligned} \tag{12}$$

$$\begin{aligned} b(t) = \ & \cos 2\gamma\sin\lambda\sin\delta\cos[2(\alpha - \phi_r - \Omega_r t)] \\ & +\frac{1}{4}\sin 2\gamma(3 - \cos 2\lambda)\sin\delta\sin[2(\alpha - \phi_r - \Omega_r t)] \\ & +\cos 2\gamma\cos\lambda\cos\delta\cos[\alpha - \phi_r - \Omega_r t] \\ & +\frac{1}{2}\sin 2\gamma\sin 2\lambda\cos\delta\sin[\alpha - \phi_r - \Omega_r t]. \end{aligned} \tag{13}$$

By means of Eqs. (10)–(13) the beam-pattern functions can be computed directly for any instant of time.

Equivalent explicit formulae for the beam-pattern functions F_+ and $F_\times$ (for the case $\zeta = \pi/2$) can be found in Ref. [26] where different angles describing the position of the gravitational-wave source in the sky and the orientation of the detector on the Earth are used. Also for the case $\zeta = \pi/2$ the functions a and b can be found in Ref. [19], where still another set of angles is used [27].

4

2.2 The phase of the gravitational-wave signal

In Appendix A we derive the time dependence of the phase of the gravitational-wave signal observed at the detector's location. We consider the significance of the corrections due to the motion of both the detector and the neutron star with respect to the the solar system barycenter (SSB) reference frame as well as the importance of relativistic corrections. On the basis of the discussion presented in Appendix A we adopt the following model of the phase of the gravitational-wave signal:

$$\Psi(t) = \Phi_0 + 2\pi \sum_{k=0}^{s} \overset{(k)}{f_0} \frac{t^{k+1}}{(k+1)!} + \frac{2\pi}{c} \mathbf{n}_0 \cdot \mathbf{r}_{\mathrm{d}}(t) \sum_{k=0}^{s} \overset{(k)}{f_0} \frac{t^k}{k!}, \tag{14}$$

where $\overset{(k)}{f_0}$ is the kth time derivative of the instantaneous frequency evaluated at $t = 0$ at the SSB, $\mathbf{n}_0$ is the constant unit vector in the direction of the star in the SSB reference frame and $\mathbf{r}_{\mathrm{d}}$ is the position vector of the detector in that frame.

The signal analysis presented in the remaining part of the paper does not depend on the number s of the spindown parameters and therefore we keep s unspecified.

We associate a coordinate system with the SSB reference frame. The x axis of the system is parallel to the x axis of the celestial sphere coordinate system, the z axis is perpendicular to the ecliptic and coincides with the orbital angular momentum vector of the Earth. In that system the unit vector $\mathbf{n}_0$ pointing towards the star has the components

$$\mathbf{n}_0 = \begin{pmatrix} 1 & 0 & 0 \\ 0 & \cos\varepsilon & \sin\varepsilon \\ 0 & -\sin\varepsilon & \cos\varepsilon \end{pmatrix} \begin{pmatrix} \cos\alpha \cos\delta \\ \sin\alpha \cos\delta \\ \sin\delta \end{pmatrix}, \tag{15}$$

where ε is the angle between ecliptic and the Earth's equator. The position vector $\mathbf{r}_{\mathrm{d}}$ of the detector has in this coordinate system the components

$$\mathbf{r}_{\mathrm{d}} = R_{ES} \begin{pmatrix} \cos(\phi_o + \Omega_o t) \\ \sin(\phi_o + \Omega_o t) \\ 0 \end{pmatrix} + R_E \begin{pmatrix} 1 & 0 & 0 \\ 0 & \cos\varepsilon & \sin\varepsilon \\ 0 & -\sin\varepsilon & \cos\varepsilon \end{pmatrix} \begin{pmatrix} \cos\lambda \cos(\phi_r + \Omega_r t) \\ \cos\lambda \sin(\phi_r + \Omega_r t) \\ \sin\lambda \end{pmatrix}, \tag{16}$$

where $R_{ES} = 1$ AU is the mean distance from the Earth's center to the SSB, R_E is the mean radius of the Earth, Ω_o is the mean orbital angular velocity of the Earth and ϕ_o is a deterministic phase which defines the position of the Earth in its orbital motion at $t = 0$. We recall that we neglect the eccentricity of the Earth's orbit and the motion of the Earth around the Earth-Moon barycenter.

Substituting Eqs. (15) and (16) into Eq. (14) one gets

$$\Psi(t) = \Phi_0 + \Phi(t), \tag{17}$$

$$\Phi(t) = 2\pi \sum_{k=0}^{s} \overset{(k)}{f_0} \frac{t^{k+1}}{(k+1)!}$$

$$+ \frac{2\pi}{c} \{ R_{ES} \left[\cos\alpha \cos\delta \cos(\phi_o + \Omega_o t) + (\cos\varepsilon \sin\alpha \cos\delta + \sin\varepsilon \sin\delta) \sin(\phi_o + \Omega_o t) \right]$$

$$+ R_E \left[\sin\lambda \sin\delta + \cos\lambda \cos\delta \cos(\alpha - \phi_r - \Omega_r t) \right] \} \sum_{k=0}^{s} \overset{(k)}{f_0} \frac{t^k}{k!}. \tag{18}$$

2.3 Wave polarization functions

We use the following two-component model of the gravitational-wave signal:

$$h(t) = h_1(t) + h_2(t), \tag{19}$$

where

$$h_1(t) = F_+(t)h_{1+}(t) + F_\times(t)h_{1\times}(t), \quad h_2(t) = F_+(t)h_{2+}(t) + F_\times(t)h_{2\times}(t), \tag{20}$$

$$h_{1+}(t) = \tfrac{1}{8} h_o \sin 2\theta \sin 2\iota \cos \Psi(t), \quad h_{2+}(t) = \tfrac{1}{2} h_o \sin^2 \theta (1 + \cos^2 \iota) \cos 2\Psi(t), \tag{21}$$

$$h_{1\times}(t) = \tfrac{1}{4} h_o \sin 2\theta \sin \iota \sin \Psi(t), \quad h_{2\times}(t) = h_o \sin^2 \theta \cos \iota \sin 2\Psi(t). \tag{22}$$

5

The beam-pattern functions F_+, $F_\times$ are given by Eqs. (10)–(13) and the phase Ψ is given by Eqs. (17) and (18).

The model of the signal defined by Eqs. (19)–(22) represents the quadrupole gravitational wave that is emitted by a freely precessing axisymmetric star. The angle θ, called the wobble angle, is the angle between the total angular momentum vector of the star and the star's axis of symmetry and ι is the angle between the total angular momentum vector of the star and the direction from the star to the Earth. The amplitude h_o is given by

$$h_o = \frac{16\pi^2 G}{c^4} \frac{\epsilon I f^2}{r}, \tag{23}$$

where f is the sum of the frequency of rotation of the star and the frequency of precession, I is the moment of inertia with respect to the rotation axis, ϵ is the poloidal ellipticity of the star and r is the distance to the star. For small wobble angle the signal h_1 is dominant. Details of the model can be found in [9]. When $\theta = \pi/2$ the h_1 component vanishes. For this special case the h_2 component is the quadrupole wave from a triaxial ellipsoid rotating about a principal axis with frequency f. In this case the amplitude h_o is again given by Eq. (23) except that ϵ is now the ellipticity of the star defined by

$$\epsilon = \frac{I_1 - I_2}{I}, \tag{24}$$

where I_1 and I_2 are the moments of inertia of the star with respect to the principal axes orthogonal to the rotation axis. This model was considered in [21].

Replacing the physical constants in Eq. (23) by their numerical values results in

$$h_o = 4.23 \times 10^{-25} d_o \left(\frac{f}{100 \text{ Hz}} \right)^2, \tag{25}$$

where

$$d_o := \left(\frac{\epsilon}{10^{-5}} \right) \left(\frac{I}{10^{45} \text{ g cm}^2} \right) \left(\frac{1 \text{ kpc}}{r} \right). \tag{26}$$

By means of Eqs. (10) and (11) the signal described by Eqs. (19)–(22) can be written in the form

$$h(t) = \sum_{i=1}^4 A_{1i}\, h_{1i}(t) + \sum_{i=1}^4 A_{2i}\, h_{2i}(t), \tag{27}$$

where the eight amplitudes A_{1i} and A_{2i} are given by

$$A_{11} = h_o \sin\zeta \sin 2\theta \left[\frac{1}{8}\sin 2\iota \cos 2\psi \cos\Phi_0 - \frac{1}{4}\sin\iota \sin 2\psi \sin\Phi_0 \right], \tag{28}$$

$$A_{12} = h_o \sin\zeta \sin 2\theta \left[\frac{1}{4}\sin\iota \cos 2\psi \sin\Phi_0 + \frac{1}{8}\sin 2\iota \sin 2\psi \cos\Phi_0 \right], \tag{29}$$

$$A_{13} = h_o \sin\zeta \sin 2\theta \left[-\frac{1}{8}\sin 2\iota \cos 2\psi \sin\Phi_0 - \frac{1}{4}\sin\iota \sin 2\psi \cos\Phi_0 \right], \tag{30}$$

$$A_{14} = h_o \sin\zeta \sin 2\theta \left[\frac{1}{4}\sin\iota \cos 2\psi \cos\Phi_0 - \frac{1}{8}\sin 2\iota \sin 2\psi \sin\Phi_0 \right], \tag{31}$$

$$A_{21} = h_o \sin\zeta \sin^2\theta \left[\frac{1}{2}(1 + \cos^2\iota)\cos 2\psi \cos 2\Phi_0 - \cos\iota \sin 2\psi \sin 2\Phi_0 \right], \tag{32}$$

$$A_{22} = h_o \sin\zeta \sin^2\theta \left[\frac{1}{2}(1 + \cos^2\iota)\sin 2\psi \cos 2\Phi_0 + \cos\iota \cos 2\psi \sin 2\Phi_0 \right], \tag{33}$$

$$A_{23} = h_o \sin\zeta \sin^2\theta \left[-\frac{1}{2}(1 + \cos^2\iota)\cos 2\psi \sin 2\Phi_0 - \cos\iota \sin 2\psi \cos 2\Phi_0 \right], \tag{34}$$

$$A_{24} = h_o \sin\zeta \sin^2\theta \left[-\frac{1}{2}(1 + \cos^2\iota)\sin 2\psi \sin 2\Phi_0 + \cos\iota \cos 2\psi \cos 2\Phi_0 \right]. \tag{35}$$

The amplitudes A_{1i} and A_{2i} depend on the parameters h_o, θ, ψ, ι, and Φ_0. They also depend on the angle ζ. The time dependent functions h_{li} have the form

$$\begin{array}{llll} h_{l1} &=& a(t)\cos l\Phi(t), & h_{l2} &=& b(t)\cos l\Phi(t), \\ h_{l3} &=& a(t)\sin l\Phi(t), & h_{l4} &=& b(t)\sin l\Phi(t), \end{array} \quad l = 1, 2, \tag{36}$$

where the functions a and b are given by Eqs. (12) and (13), respectively, and Φ is the phase given by Eq. (18). The modulation amplitudes a and b depend on the right ascension α and the declination δ of the source (they also depend on the angles λ and γ). The phase Φ depends on the frequency f_0, s spindown parameters $\overset{(k)}{f_0}$ ($k = 1, \ldots, s$), and on the angles α, δ. We call parameters f_0, $\overset{(k)}{f_0}$, α, δ the *phase parameters*. Moreover the phase Φ depends on the latitude λ of the detector. The whole signal h depends on $8 + s$ unknown parameters: $h_o, \theta, \psi, \iota, \Phi_0, \alpha, \delta, f_0, \overset{(k)}{f_0}$.

It is useful to consider the frequency domain characteristics of our gravitational-wave signal. The signal consists of two components with carrier frequencies f_0 and $2f_0$ that are both amplitude and phase modulated. The amplitude modulation, determined by functions a and b, splits each of the two components into five lines corresponding to frequencies $f_0 - 2f_r$, $f_0 - f_r$, f_0, $f_0 + f_r$, $f_0 + 2f_r$, where f_r is the frequency of rotation of Earth ($f_r \simeq 10^{-5}$ Hz) and the same for frequency $2f_0$. The frequency modulation broadens the lines. For the extreme case of the gravitational-wave frequency of 10^3 Hz, the spindown age $\tau = 40$ years, and the observation time $T_o = 120$ days the maximum frequency shifts due to the neutron star spindown, Earth orbital motion and Earth diurnal motion are respectively $\sim$8 Hz, $\sim$0.1 Hz, and $\sim 10^{-3}$ Hz. As an example in Figure 1 we have plotted the power spectrum of the noise-free response of a detector located near Hannover to the gravitational wave from the Crab pulsar. We took only the component h_2 with twice the rotational frequency. We have generated a 24-day long signal.

3 Optimal filtering for the amplitude modulated signal

3.1 Maximum likelihood detection

The signal given by Eq. (27) will be buried in the noise of a detector. Thus we are faced with the problem of detecting the signal and estimating its parameters. A standard method is the method of *maximum likelihood detection* which consists of maximizing the likelihood function Λ with respect to the parameters of the signal. If the maximum of Λ exceeds a certain threshold calculated from the false alarm probability that we can afford we say that the signal is detected. The values of the parameters that maximize Λ are said to be the *maximum likelihood (ML) estimators* of the parameters of the signal. The magnitude of the maximum of Λ determines the probability of detection of the signal.

We assume that the noise n in the detector is an additive, stationary, Gaussian, and zero-mean continuous random process. Then the data x (if the signal h is present) can be written as

$$x(t) = n(t) + h(t). \tag{37}$$

The log likelihood function has the form

$$\log \Lambda = (x|h) - \frac{1}{2}(h|h), \tag{38}$$

where the scalar product $(\,\cdot\,|\,\cdot\,)$ is defined by

$$(x|y) := 4\Re \int_0^\infty \frac{\tilde{x}(f)\tilde{y}^*(f)}{S_h(f)} df, \tag{39}$$

where $\tilde{}$ denotes the Fourier transform, $*$ is complex conjugation, and S_h is the *one-sided* spectral density of the detector's noise.

The gravitational-wave signal given by Eq. (27) consists of two narrowband components around the frequencies f_0 and $2f_0$ and therefore to a very good accuracy the likelihood ratio is given by

$$\log \Lambda \cong (x|h_1) - \frac{1}{2}(h_1|h_1) + (x|h_2) - \frac{1}{2}(h_2|h_2). \tag{40}$$

This suggests that we consider the two components of the response function (27) as two independent signals. Let us take the first component h_1 of the signal. We can assume that over the bandwidth of the signal $S_h(f)$ is nearly constant and equal to $S_h(f_0)$ where f_0 is the frequency of the signal h_1 at $t = 0$. Thus in our case the above scalar product can be approximated by

$$(x|h_1) \cong \frac{2}{S_h(f_0)} \int_{-T_o/2}^{T_o/2} x(t)h_1(t)\, dt, \tag{41}$$

7

where T_o is the observation time and where the observation interval is $[-T_o/2, T_o/2]$. It is useful to introduce the following scalar product

$$(x||y) := \frac{2}{T_o} \int_{-T_o/2}^{T_o/2} x(t)y(t)\, dt. \tag{42}$$

As long as the detector's noise is stationary over the observation period, this is a good scalar product. In realistic observations, the detector's noise will vary slowly during the observation period. We do not treat this important issue in this paper.

The log likelihood function for this signal is approximately given by

$$\log \Lambda_1 \cong \frac{T_o}{S_h(f_0)} \left[(x||h_1) - \frac{1}{2}(h_1||h_1) \right]. \tag{43}$$

The maximum likelihood estimators can be found by maximizing the following *normalized log likelihood function*

$$\log \Lambda_1' = (x||h_1) - \frac{1}{2}(h_1||h_1). \tag{44}$$

The normalized log likelihood function does not involve explicitly the spectral density of the noise in the detector.

The signal h_1 depends linearly on four amplitudes A_{1i}. The amplitudes depend on the five unknown parameters h_o, θ, ψ, ι, and Φ_0 and are independent. The likelihood equations for the amplitudes A_{1i} are given by

$$\frac{\partial \ln \Lambda_1'}{\partial A_{1i}} = 0, \quad i = 1, \ldots, 4. \tag{45}$$

One easily finds that in our case the above set of equations is equivalent to the following set of linear algebraic equations

$$\sum_{j=1}^{4} \mathcal{M}_{ij} A_{1j} = (x||h_{1i}), \quad i = 1, \ldots, 4, \tag{46}$$

where the components $\mathcal{M}_{ij}$ of the 4×4 matrix $\mathcal{M}$ are given by

$$\mathcal{M}_{ij} := (h_{1i}||h_{1j}). \tag{47}$$

Since over a typical observation time T_o the phase Φ will have very many oscillations, then to a very good accuracy we have

$$(h_{11}||h_{13}) \cong 0, \quad (h_{11}||h_{14}) \cong 0, \quad (h_{12}||h_{13}) \cong 0, \quad (h_{12}||h_{14}) \cong 0, \tag{48}$$

and also

$$\begin{array}{rclcl}
(h_{11}||h_{11}) & \cong & (h_{13}||h_{13}) & \cong & \frac{1}{2}A, \\
(h_{12}||h_{12}) & \cong & (h_{14}||h_{14}) & \cong & \frac{1}{2}B, \\
(h_{11}||h_{12}) & \cong & (h_{13}||h_{14}) & \cong & \frac{1}{2}C,
\end{array} \tag{49}$$

where $A := (a||a)$, $B := (b||b)$, $C := (a||b)$. With these approximations the matrix $\mathcal{M}$ is given by

$$\mathcal{M} = \left(\begin{array}{cc} \mathcal{C} & \mathcal{O} \\ \mathcal{O} & \mathcal{C} \end{array} \right), \tag{50}$$

where $\mathcal{O}$ is a zero 2 by 2 matrix and $\mathcal{C}$ equals

$$\mathcal{C} = \frac{1}{2} \left(\begin{array}{cc} A & C \\ C & B \end{array} \right). \tag{51}$$

Thus $\mathcal{M}$ splits into two identical 2×2 matrices. Assuming that $a \neq b$, $A \neq 0$ and $B \neq 0$ the explicit expressions for maximum likelihood estimators $\widehat{A}_{1i}$ of the amplitudes A_{1i} are readily obtained and they are given by

$$\begin{array}{rcl}
\widehat{A}_{11} & = & 2\dfrac{B(x||h_{11}) - C(x||h_{12})}{D}, \\[2mm]
\widehat{A}_{12} & = & 2\dfrac{A(x||h_{12}) - C(x||h_{11})}{D}, \\[2mm]
\widehat{A}_{13} & = & 2\dfrac{B(x||h_{13}) - C(x||h_{14})}{D}, \\[2mm]
\widehat{A}_{14} & = & 2\dfrac{A(x||h_{14}) - C(x||h_{13})}{D},
\end{array} \tag{52}$$

where D is defined by

$$D = AB - C^2. \tag{53}$$

The second partial derivatives of the log likelihood function w.r.t. A_{1i} are given by

$$\frac{\partial^2 \ln \Lambda_1'}{\partial A_{1i} \partial A_{1j}} = -\mathcal{M}_{ij}. \tag{54}$$

Since $a \neq b$ it follows from Schwarz inequality that $D > 0$. Thus as $A > 0$ and $B > 0$ the matrix $\mathcal{M}$ is positive-definite. Therefore the extrema of the log likelihood function w.r.t. A_{1i} are the local maxima. The above ML estimators of the amplitudes A_{1i} are substituted for the amplitudes A_{1i} in the likelihood function (44) giving the reduced normalized likelihood function $\Lambda_1'' = \exp(\mathcal{F}_1)$ where $\mathcal{F}_1$ is given by

$$\mathcal{F}_1 = \frac{B(x||h_{11})^2 + A(x||h_{12})^2 - 2C(x||h_{11})(x||h_{12})}{D}$$
$$+ \frac{B(x||h_{13})^2 + A(x||h_{14})^2 - 2C(x||h_{13})(x||h_{14})}{D}. \tag{55}$$

Thus to obtain the maximum likelihood estimators of the parameters of the signal one first finds the maximum of the functional $\mathcal{F}_1$ with respect to the frequency, the spindown parameters and the angles α and δ and then one calculates the estimators of the amplitudes A_{1i} from the analytic formulae (52) with the correlations $(x||h_{1i})$ evaluated at the values of the parameters obtained by the maximization of the functional $\mathcal{F}_1$. Thus we see that filtering for the gravitational-wave signal from a neutron star requires *four linear* filters. Efficient numerical methods to calculate the statistics $\mathcal{F}_1$ are discussed in Section 3.4.

Exactly the same procedure applies to the second component of the signal. The formulae for the estimators of the amplitudes A_{2i} and the normalized reduced statistics $\mathcal{F}_2$ are obtained from the above formulae by replacing h_{1i} by h_{2i}.

To consider the optimal detection of the whole two-component signal we need to remember that the eight amplitudes A_{li} are not independent. They depend on five parameters: h_o, θ, ψ, ι, and Φ_0. To find the maximum likelihood estimators of the independent five parameters we would have to maximize the total likelihood function (given by Eq. (40)) with respect to these parameters. This however leads to an intractable set of nonlinear algebraic equations which would have to be solved numerically, thereby increasing the computational cost of the search for the signal. Instead we propose the following procedure.

We form the statistics

$$\mathcal{F} = \frac{T_o}{S_h(f_0)}\mathcal{F}_1 + \frac{T_o}{S_h(2f_0)}\mathcal{F}_2. \tag{56}$$

This is just the reduced likelihood function assuming that the eight amplitudes are independent. We first maximize the functional $\mathcal{F}$ with respect to the frequency, spindown parameters and angles α and δ and we calculate the eight amplitudes from the analytic formulae. We then find the estimators of the five independent parameters from the estimators of the amplitudes by least-squares method. We use the inverse of Fisher matrix for the covariance matrix in the least-squares method. We shall consider this problem in Paper IV.

To announce the detection of the signal the functional $\mathcal{F}$ must exceed a certain threshold calculated on the basis of the false alarm probability that one can afford. Once $\mathcal{F}$ is above the threshold its magnitude determines the probability of detection of the signal. Consequently we need to determine the probability density function of $\mathcal{F}$ both when the signal is absent and present.

We shall first calculate these probabilities when the parameters which $\mathcal{F}$ depends on are known i.e. when the filters h_{li} are known functions of time. We shall then explain how to obtain approximate formulae for the false alarm and the detection probabilities when parameters of the filters are unknown.

3.2 Detection statistics

We shall first consider the probability density function of the normalized reduced functional $\mathcal{F}_1$. Let us suppose that filters h_{1i} are known functions of time, i.e. the phase parameters f_0, $\overset{(k)}{f_0}$, α, δ are known, and let us define the following random variables

$$x_{1i} := (x||h_{1i}), \quad i = 1, \ldots, 4. \tag{57}$$

Since x is a Gaussian random process the random variables x_{1i} being linear in x are also Gaussian. Let $E_0\{x_{1i}\}$ and $E_1\{x_{1i}\}$ be respectively the means of x_{1i} when the signal is absent and when the signal is present. One easily gets

$$E_0\{x_{1i}\} = 0, \quad i = 1, \ldots, 4, \tag{58}$$

and

$$m_{11} \;\; := \;\; E_1\{x_{11}\} = \frac{1}{2}(AA_{11} + CA_{12}), \tag{59}$$

$$m_{12} \;\; := \;\; E_1\{x_{12}\} = \frac{1}{2}(CA_{11} + BA_{12}), \tag{60}$$

$$m_{13} \;\; := \;\; E_1\{x_{13}\} = \frac{1}{2}(AA_{13} + CA_{14}), \tag{61}$$

$$m_{14} \;\; := \;\; E_1\{x_{14}\} = \frac{1}{2}(CA_{13} + BA_{14}). \tag{62}$$

One finds that the covariance matrix for the random variables x_{1i} is the same whether the signal is present or not and it splits into two identical 2 by 2 covariance matrices $\mathcal{C}$ for the pairs (x_{11}, x_{12}) and (x_{13}, x_{14}) of random variables where $\mathcal{C}$ is given by Eq. (51). Hence the covariance matrix is exactly equal to the matrix $\mathcal{M}$ given by Eq. (50) above.

Thus in effect (x_{11}, x_{12}) and (x_{13}, x_{14}) are pairs of correlated Gaussian random variables, with pairs being independent of each other. For Gaussian variables their first two moments determine uniquely their probability density function (pdf). Consequently the joint probability density function $p(x_{11}, x_{12}, x_{13}, x_{14})$ is equal to a product $p_a(x_{11}, x_{12})\, p_b(x_{13}, x_{14})$, where p_a and p_b are bivariate Gaussian pdfs with the same covariance matrix $\mathcal{C}$:

$$p_a(x_{11}, x_{12}) = \frac{1}{\pi\sqrt{D}} \exp\left(-\frac{B\tilde{x}_{11}^2 + A\tilde{x}_{12}^2 - 2C\tilde{x}_{11}\tilde{x}_{12}}{D}\right), \tag{63}$$

and a similar formula for $p_b(x_{13}, x_{14})$, where $\tilde{x}_{1i} = x_{1i}$ when the signal is absent and $\tilde{x}_{1i} = x_{1i} - m_{1i}$ when the signal is present. It is interesting to note that when the signal is absent the joint pdf p_0 is simply given by

$$p_0 = \frac{1}{\pi^2 D} \exp(-\mathcal{F}_1), \tag{64}$$

where $\mathcal{F}_1$ is our optimal statistics. We want to find the pdf of $\mathcal{F}_1$ when the signal is absent and present. We first decorrelate the variables x_{1i}. For the case of Gaussian variables this can always be done by means of a linear transformation. Let us consider the following transformation matrix $\mathcal{L}$

$$\mathcal{L} = \begin{pmatrix} \mathcal{N} & \mathcal{O} \\ \mathcal{O} & \mathcal{N} \end{pmatrix}, \tag{65}$$

where $\mathcal{O}$ is a zero 2 by 2 matrix and $\mathcal{N}$ is given by

$$\mathcal{N} = \begin{pmatrix} 1/\sqrt{A + C\sqrt{A/B}} & 1/\sqrt{B + C\sqrt{B/A}} \\ -1/\sqrt{A - C\sqrt{A/B}} & 1/\sqrt{B - C\sqrt{B/A}} \end{pmatrix}. \tag{66}$$

Let us introduce new random variables z_{1i} ($i = 1, \ldots, 4$) such that $z_{1i} = \sum_{j=1}^{4} \mathcal{L}_{ij} x_{1j}$. In the new variables the pdf takes the form

$$p(z_{11}, z_{12}, z_{13}, z_{14}) = \frac{1}{(2\pi)^2} \exp\left[-\frac{1}{2}\left(\tilde{z}_{11}^2 + \tilde{z}_{12}^2 + \tilde{z}_{13}^2 + \tilde{z}_{14}^2\right)\right]. \tag{67}$$

Thus z_{1i} are independent Gaussian random variables with unit variances. When the signal is absent we have $\tilde{z}_{1i} = z_{1i}$ and when the signal is present $\tilde{z}_{1i} = z_{1i} - m'_{1i}$, where $m'_{1i} = \sum_{j=1}^{4} \mathcal{L}_{ij} m_{1j}$. The functional $\mathcal{F}_1$ in the new variables is given by

$$\mathcal{F}_1 = \frac{1}{2}\left(z_{11}^2 + z_{12}^2 + z_{13}^2 + z_{14}^2\right). \tag{68}$$

10

The probability density distributions of $\mathcal{F}_1$ both when the signal is absent and present are well known. When the signal is absent $2\mathcal{F}_1$ has a χ^2 distribution with 4 degrees of freedom and when signal is present it has a noncentral χ^2 distribution with 4 degrees of freedom and noncentrality parameter $\lambda = \sum_{i=1}^{4}(m'_{1i})^2$.

In exactly the same way one obtains the pdf for the normalized reduced functional for the second component of the signal. The second component depends on four amplitudes A_{2i}. The decorrelation is achieved by the same matrix $\mathcal{L}$. Let us denote the four decorrelated random variables for the second component by z_{2i} and their means by m'_{2i} $(i = 1, \ldots, 4)$.

To obtain the pdf of the statistics $\mathcal{F}$ for the detection of the two-component signal it is convenient to introduce the following normalized random variables z_i^n:

$$z_i^n = z_{1i}\sqrt{\frac{T_o}{S_h(f_0)}}, \quad z_{4+i}^n = z_{2i}\sqrt{\frac{T_o}{S_h(2f_0)}}, \quad i = 1, \ldots, 4, \tag{69}$$

so that each random variable z_i^n has a unit variance. Consequently $2\mathcal{F} = \sum_{i=1}^{8}(z_i^n)^2$ has a χ^2 distribution with 8 degrees of freedom when the signal is absent and noncentral χ^2 with 8 degrees of freedom when signal is present. The noncentrality parameter λ is given by

$$\lambda = \frac{T_o}{S_h(f_0)}\sum_{i=1}^{4} m'_{1i} + \frac{T_o}{S_h(2f_0)}\sum_{i=1}^{4} m'_{2i}. \tag{70}$$

After some algebra one finds that $\lambda = d^2$ where

$$d := \sqrt{(h|h)}. \tag{71}$$

The quantity d is called the *optimal signal-to-noise ratio*. It is the maximum signal-to-noise ratio that can be achieved for a signal in additive noise with the *linear* filter [31]. This fact does not depend on the statistics of the noise.

Consequently the pdfs p_0 and p_1 when respectively the signal is absent and present are given by

$$p_0(\mathcal{F}) = \frac{\mathcal{F}^3}{6}\exp(-\mathcal{F}), \tag{72}$$

$$p_1(d, \mathcal{F}) = \frac{(2\mathcal{F})^{3/2}}{d^3}I_3\left(d\sqrt{2\mathcal{F}}\right)\exp\left(-\mathcal{F} - \frac{1}{2}d^2\right), \tag{73}$$

where I_3 is the modified Bessel function of the first kind and order 3. The false alarm probability P_F is the probability that $\mathcal{F}$ exceeds a certain threshold $\mathcal{F}_o$ when there is no signal. In our case we have

$$P_F(\mathcal{F}_o) := \int_{\mathcal{F}_o}^{\infty} p_0(\mathcal{F})\,d\mathcal{F} = \left(1 + \mathcal{F}_o + \frac{1}{2}\mathcal{F}_o^2 + \frac{1}{6}\mathcal{F}_o^3\right)\exp(-\mathcal{F}_o). \tag{74}$$

The probability of detection P_D is the probability that $\mathcal{F}$ exceeds the threshold $\mathcal{F}_o$ when the signal-to-noise ratio is equal to d:

$$P_D(d, \mathcal{F}_o) := \int_{\mathcal{F}_o}^{\infty} p_1(d, \mathcal{F})\,d\mathcal{F}. \tag{75}$$

Thus we see that when the noise in the detector is Gaussian and the phase parameters are known the probability of detection of the signal depends on a single quantity: the optimal signal-to-noise ratio d. In view of its importance we shall investigate in detail the dependence of the optimal signal-to-noise ratio on the parameters of the signal in the next section.

Let us introduce a vector parameter $\theta_i^{ph} = (f_0, \overset{(k)}{f_0}, \alpha, \delta)$ denoting the phase parameters. When parameters θ_i^{ph} are known the optimal statistics $\mathcal{F}$ is a random variable with probability density functions given above. When the phase parameters are not known we can think of $\mathcal{F}$ as a multi-dimensional random process $\mathcal{F}(\theta_i^{ph})$ with dimension equal to the number of phase parameters. Such a process is called *random field*. For each realization $x(t)$ of the data random process the corresponding realization of the random field is obtained by evaluating $\mathcal{F}$ for filters h_{li} with continuously varying parameters θ_i^{ph}. For such a process we can define the autocorrelation function $\mathbf{C}$ just in the same way as we define the autocorrelation function for a one parameter random process:

$$\mathbf{C} = E[\mathcal{F}(\theta_i^{ph})\mathcal{F}(\theta_i'^{ph})]. \tag{76}$$

Let us first assume that the signal is absent, i.e. $x(t) = n(t)$. For many cases of interest the autocorrelation function will tend to zero as the differences $\Delta_i = \theta_i'^{ph} - \theta_i^{ph}$ increase. Thus we can divide the parameter space into elementary cells such that in each cell $\mathbf{C}$ is appreciably different from zero. The realizations of the random field within a cell will be correlated (dependent) whereas realizations of the random field within each cell and outside the cell are almost uncorrelated (independent). Thus the number of cells covering the parameter space estimates the number of independent samples of the random field. For some signals the autocorrelation function will depend only on the differences Δ_i and not on the absolute values of the parameters. Then the random field $\mathcal{F}$ is called a *homogeneous random field*. In this case one can introduce the notion of the correlation hyperellipse as a generalization of the correlation time of a stationary process and estimate the area of the elementary cell by the area of the correlation hyperellipse. For the general case of a random field the number of elementary cells N_c can be estimated from Owen's formula [29, 21] with an appropriate choice of the mismatch parameter μ and for the case of a homogeneous random field from a formula proposed by one of us [22]. For the parameter values in each cell the probability distribution of $\mathcal{F}(\theta_i^{ph})$ can be approximated by probability $p_0(\mathcal{F})$ given by Eq. (72). Thus the probability distribution of $\mathcal{F}$ is given by product of N_c pdfs $p_0(\mathcal{F})$. The probability that $\mathcal{F}$ does not exceed the threshold $\mathcal{F}_o$ in a given cell is $1 - P_F(\mathcal{F}_o)$, where $P_F(\mathcal{F}_o)$ is given by Eq. (74). The probablity that $\mathcal{F}$ does not exceed the threshold $\mathcal{F}_o$ in all the N_c cells is $[1 - P_F(\mathcal{F}_o)]^{N_c}$. The probability P_F^T that $\mathcal{F}$ exceeds $\mathcal{F}_o$ in *one or more cell* is given by

$$P_F^T(\mathcal{F}_o) = 1 - [1 - P_F(\mathcal{F}_o)]^{N_c}. \tag{77}$$

This is the false alarm probability when the phase parameters are unknown. When $P_F(\mathcal{F}_o) \ll 1$ and $N_c P_F(\mathcal{F}_o) < 1$ we have $P_F^T \cong N_c P_F(\mathcal{F}_o)$. When the signal is present a precise calculation of the pdf of $\mathcal{F}$ would be very difficult because the presence of the signal makes the data random process $x(t)$ non-stationary. As a first approximation we can approximate the probability of detection of the signal when parameters are unknown by the probability of detection when the parameters of the signal are known [given by Eq. (75)]. This approximation assumes that when the signal is present the true values of the phase parameters fall within the cell where $\mathcal{F}$ has a maximum. This approximation will be the better the higher the signal-to-noise ratio d. An accurate probability of detection can be obtained by numerical simulations. Parametric plot of probability of detection vs. probability of false alarm with optimal signal-to-noise ratio d as a parameter is called the *receiver operating characteristic* (ROC). Detailed calculations of the number of cells N_c and false alarm probabilities as well as plots of receiver operating characteristic for the case of the signal considered here will be given in Paper III.

The above reasoning is a generalization to the case of many parameters of the idea of an *effective sampling rate* introduced by one of us [15] and further developed in [30]. Related ideas can also be found in Ref. [32].

For large signal-to-noise ratios, the rms errors of the estimators of the parameters of the signal are approximately given by the square roots of the diagonal elements of the inverse of the Fisher information matrix Γ with the components given by

$$\Gamma_{ij} = \left(\left. \frac{\partial h}{\partial \theta_i} \right| \frac{\partial h}{\partial \theta_j} \right). \tag{78}$$

We shall study these errors in detail in Paper II. For smaller signal-to-noise ratios (e.g. $\lesssim 10$) the errors are larger (see Ref. [33] for a discussion in the context of coalescing binaries).

3.3   Signal-to-noise ratio

In this subsection we use the following models of the noise spectral densities S_h in the individuals detectors. The noise curves for the VIRGO and the initial/advanced LIGO detectors are taken from [35], and the noise curve for the TAMA300 detector is taken from [6, 36]. Wideband and narrowband versions of the GEO600 detector noise are based on [37].

The optimal signal-to-noise ratio d is given by the formula (71):

$$d := \sqrt{(h|h)}. \tag{79}$$

The gravitational-wave signal defined by Eqs. (19)–(22) consists of two narrowband components around the frequencies f_0 and $2f_0$ and therefore to a very good accuracy the signal-to-noise ratio (79) for that

signal can be written as

$$d \cong \sqrt{d_1^2 + d_2^2},\tag{80}$$

where d_1 and d_2 are the signal-to-noise ratios for the individual components of the signal. They are given by

$$d_1 \quad := \quad \sqrt{(h_1|h_1)} \cong \left\{ \frac{2}{S_h(f_0)} \int_{-T_o/2}^{T_o/2} [h_1(t)]^2 \, dt \right\}^{1/2},\tag{81}$$

$$d_2 \quad := \quad \sqrt{(h_2|h_2)} \cong \left\{ \frac{2}{S_h(2f_0)} \int_{-T_o/2}^{T_o/2} [h_2(t)]^2 \, dt \right\}^{1/2}.\tag{82}$$

We substitute Eqs. (19)–(22) to Eqs. (81)–(82) and drop out terms which oscillate around zero with multiples of the frequency f_0. We obtain

$$d_1^2 \quad \cong \quad \left[\frac{1}{64} \sin^2 2\iota \int_{-T_o/2}^{T_o/2} F_+^2 \, dt + \frac{1}{16} \sin^2 \iota \int_{-T_o/2}^{T_o/2} F_\times^2 \, dt \right] \frac{h_o^2 \sin^2 2\theta}{S_h(f_0)},\tag{83}$$

$$d_2^2 \quad \cong \quad \left[\frac{1}{4} \left(1 + \cos^2 \iota\right)^2 \int_{-T_o/2}^{T_o/2} F_+^2 \, dt + \cos^2 \iota \int_{-T_o/2}^{T_o/2} F_\times^2 \, dt \right] \frac{h_o^2 \sin^4 \theta}{S_h(2f_0)}.\tag{84}$$

After performing integrations in (83) and (84) we get:

$$d_1^2 \quad \cong \quad [A_1(\delta, \psi, \iota) T_o + B_1(\alpha, \delta, \psi, \iota; T_o)] \sin^2 \zeta \frac{h_o^2 \sin^2 2\theta}{S_h(f_0)},\tag{85}$$

$$d_2^2 \quad \cong \quad [A_2(\delta, \psi, \iota) T_o + B_2(\alpha, \delta, \psi, \iota; T_o)] \sin^2 \zeta \frac{h_o^2 \sin^4 \theta}{S_h(2f_0)}.\tag{86}$$

The functions B_1 and B_2 are periodic in the observation time T_o with the period of two sidereal days (cf. Eq. (136) from Appendix B). For simplicity we suppress the explicit dependence of the functions A_k and B_k on the angles λ and γ. Detailed expressions for the functions A_k and B_k are given in Appendix B.

For the observation times T_o longer than several days the signal-to-noise ratios d_1, d_2, and d are dominated by terms proportional to the square root of the observation time T_o. This can be seen in Figures 2 and 3.

The signal-to-noise ratios d_1^2 and d_2^2 are complicated functions of the angles α, δ, ψ, ι, and θ. We have studied the different averages of d_1^2 and d_2^2 over these angles. Averaging is performed according to the definition:

$$\langle \cdots \rangle_{\alpha, \delta, \psi, \iota, \theta} := \frac{1}{2\pi} \int_0^{2\pi} d\alpha \times \frac{1}{2} \int_{-1}^{1} d\sin\delta \times \frac{1}{2\pi} \int_0^{2\pi} d\psi \times \frac{1}{2} \int_{-1}^{1} d\cos\iota \times \frac{1}{\pi} \int_0^{\pi} d\theta \, (\cdots).\tag{87}$$

Note that because $\delta \in [-\pi/2, \pi/2]$ integration over $\sin\delta$ rather than $\cos\delta$ is involved in Eq. (87).

Averaging over the angle α discards the oscillatory parts B_1 and B_2 of the signal-to-noise ratios d_1^2 and d_2^2:

$$\langle d_1^2 \rangle_\alpha \quad \cong \quad A_1(\delta, \psi, \iota) \sin^2 \zeta \frac{h_o^2 T_o \sin^2 2\theta}{S_h(f_0)},\tag{88}$$

$$\langle d_2^2 \rangle_\alpha \quad \cong \quad A_2(\delta, \psi, \iota) \sin^2 \zeta \frac{h_o^2 T_o \sin^4 \theta}{S_h(2f_0)}.\tag{89}$$

Further averaging over the orientation angles ψ and ι gives

$$\langle d_1^2 \rangle_{\alpha, \psi, \iota} \quad \cong \quad \frac{1}{20} e_2(\delta) \sin^2 \zeta \frac{h_o^2 T_o \sin^2 2\theta}{S_h(f_0)},\tag{90}$$

$$\langle d_2^2 \rangle_{\alpha, \psi, \iota} \quad \cong \quad \frac{4}{5} e_2(\delta) \sin^2 \zeta \frac{h_o^2 T_o \sin^4 \theta}{S_h(2f_0)}.\tag{91}$$

The function e_2 (its definition can be found in Appendix B) in the above equations is a fair representation of the average sensitivity of a detector at a given location. It depends on the declination δ of the gravitational-wave source as well as on the latitude λ of the detector's site and the angle γ describing the orientation of its arms. The product $e_2(\delta)\sin^2\zeta$ is plotted against the declination δ for different detectors in Figure 4.

Averaging over the angles α, δ, ψ, and ι yields results which do not depend on the position of the detector on the Earth and on the orientation of its arms:

$$\langle d_1^2 \rangle_{\alpha,\delta,\psi,\iota} \cong \frac{1}{100}\sin^2\zeta \frac{h_o^2 T_o \sin^2 2\theta}{S_h(f_0)}, \tag{92}$$

$$\langle d_2^2 \rangle_{\alpha,\delta,\psi,\iota} \cong \frac{4}{25}\sin^2\zeta \frac{h_o^2 T_o \sin^4 \theta}{S_h(2f_0)}. \tag{93}$$

For the special case of the model of neutron star as a triaxial ellipsoid the angle $\theta = \pi/2$ and then the contribution d_1^2 to the signal-to-noise ratio vanishes. However for small angles θ the term d_1^2 may dominate over the term d_2^2. The averaging of the above formulae over the angle θ gives

$$\langle d_1^2 \rangle_{\alpha,\delta,\psi,\iota,\theta} \cong \frac{1}{200}\sin^2\zeta \frac{h_o^2 T_o}{S_h(f_0)}, \tag{94}$$

$$\langle d_2^2 \rangle_{\alpha,\delta,\psi,\iota,\theta} \cong \frac{3}{50}\sin^2\zeta \frac{h_o^2 T_o}{S_h(2f_0)}. \tag{95}$$

We observe that when the noise spectral density at frequencies f_0 and $2f_0$ is the same the average (95) of d_2^2 is more than one order of magnitude greater than the average (94) of d_1^2.

We have studied the distribution of the signal-to-noise ratios d_1, d_2, and d over the angles α, δ, ψ, ι, and θ with the aid of the Monte Carlo simulations for the observation time $T_o = 120$ days. For each case we have generated 10000 sets of angles according to the probability measure defined by the right-hand side of Eq. (87). We have assumed that the parameter d_o given by Eq. (26) is equal to 1. The results are shown in Figures 5–7 where we have plotted cumulative distribution functions of the simulated signal-to-noise ratios d_1, d_2, and d for the initial/advanced Hanford, initial/advanced Livingston, VIRGO, GEO600, and TAMA300 detectors. We have performed simulations for two gravitational wave frequencies f_0: 100 Hz and 500 Hz. The shapes of the distributions of the signal-to-noise ratios d_1 and d_2 do not depend on the frequency f_0 (cf. Eqs. (81)–(82)) and will be the same for nonaxisymmetries generated by different physical mechanism e.g. for the case of CFS instability.

In Table 2 we have given the means and the quartiles for the Monte Carlo simulated cumulative distribution functions of the signal-to-noise ratios d_1, d_2, and d for the individual detectors.

From Figures 5, 6, and Table 2 we see that the simulated distributions of the signal-to-noise ratios d_1, d_2, and d depend weakly on the position of the detector on the Earth and on the orientation of its arms (cf. plots and data for the initial/advanced Hanford and Livingston detectors). This is related to the fact that the averages (92) and (93) are idependent of the position of the detector on the Earth and of the orientation of its arms.

3.4   Data analysis method

It is important to calculate the optimum statistics as efficiently as possible. One way to achieve this is to take advantage of the speed of the *fast Fourier transform* (FFT). Let us consider first the normalized reduced functional $\mathcal{F}_1$. One observes that the phase Φ of the signal can be written as (cf. Eq. (18))

$$\Phi(t) = 2\pi f_0[t + \Phi_m(t;\alpha,\delta)] + \Phi_s(t; \overset{(k)}{f_0}, \alpha, \delta), \tag{96}$$

where functions Φ_m and Φ_s do not depend on the frequency parameter f_0. Let us define the following two integrals:

$$F_{1a} = \int_{-T_o/2}^{T_o/2} x(t)a(t)\exp[-i\Phi_s(t)]\exp\left\{-i2\pi f_0[t + \Phi_m(t)]\right\} dt, \tag{97}$$

$$F_{1b} = \int_{-T_o/2}^{T_o/2} x(t)b(t)\exp[-i\Phi_s(t)]\exp\left\{-i2\pi f_0[t + \Phi_m(t)]\right\} dt. \tag{98}$$

14

detector		$f_0 = 100$ Hz				$f_0 = 500$ Hz			
		mean	$q_{0.25}$	$q_{0.5}$	$q_{0.75}$	mean	$q_{0.25}$	$q_{0.5}$	$q_{0.75}$
GEO600 wideband noise	d_1	0.70	0.37	0.72	1.0	14.	7.5	15.	21.
	d_2	3.1	0.79	2.7	4.7	21.	5.4	18.	32.
	d	3.2	1.1	2.9	4.7	28.	17.	28.	37.
GEO600 narrowband noise	d_1	–	–	–	–	1.2	0.64	1.3	1.8
	d_2	–	–	–	–	180.	47.	160.	280.
	d	–	–	–	–	180.	47.	160.	280.
initial Hanford	d_1	2.8	1.5	2.9	4.2	48.	25.	49.	70.
	d_2	12.	3.2	11.	19.	72.	19.	63.	110.
	d	13.	4.7	12.	19.	95.	56.	96.	120.
advanced Hanford	d_1	89.	46.	90.	130.	480.	250.	490.	700.
	d_2	140.	37.	120.	210.	720.	190.	630.	1100.
	d	180.	100.	180.	240.	950.	560.	960.	1200.
initial Livingston	d_1	2.9	1.5	3.0	4.3	48.	25.	50.	71.
	d_2	12.	3.2	11.	19.	72.	19	64.	110.
	d	13.	4.8	12.	19.	95.	58.	97.	120.
advanced Livingston	d_1	89.	47.	92.	130.	480.	260.	500.	720.
	d_2	140.	37.	130.	220.	720.	190.	640.	1100.
	d	180.	110.	180.	240.	950.	580.	970.	1200.
VIRGO	d_1	1.5	0.78	1.5	2.2	46.	24.	48.	68.
	d_2	5.8	1.5	5.2	8.9	86.	22.	76.	130.
	d	6.2	2.3	5.7	9.0	110.	57.	100.	140.
TAMA300	d_1	0.094	0.049	0.098	0.14	13.	6.9	14.	19.
	d_2	1.1	0.28	0.97	1.7	29.	7.3	25.	44.
	d	1.1	0.30	0.98	1.7	34.	17.	33.	46.
initial LIGO/VIRGO network	d_1	4.3	2.3	4.5	6.4	82.	43.	86.	120.
	d_2	19.	4.8	17.	28.	130.	35.	120.	200.
	d	20.	7.1	18.	29.	170.	100.	170.	230.

Table 2: The means and the quartiles for the Monte Carlo simulated distribution functions of the signal-to-noise ratios d_1, d_2, and d for the individual detectors and for the three detector network of the VIRGO and two initial LIGO detectors. For the GEO600 detector we use two noise curves: wideband and narrowband tuned to 1 kHz with the bandwidth of 30 Hz. We assume that star's ellipticity is 10^{-5}, its moment of inertia w.r.t. the rotation axis is 10^{45} g cm^2 and its distance from the Earth is 1 kpc. Quantile q_x gives a value z_x of random variable z such that probability that $z < z_x$ is less than or equal to x. The quantile values at $x = 0.25$, 0.5, and 0.75 are called the quartiles.

One can write the statistics $\mathcal{F}_1$ in terms of the above two integrals as:

$$\mathcal{F}_1 = \frac{4}{T_o^2} \frac{B|F_{1a}|^2 + A|F_{1b}|^2 - 2C\Re(F_{1a}F_{1b}^*)}{D}. \tag{99}$$

We can introduce a new time coordinate t_b:

$$t_b(t) = t + \Phi_m(t). \tag{100}$$

From the explicit expression for the phase Φ given by Eq. (18) the time shift Φ_m and its time derivative $\dot{\Phi}_m$ can be estimated by

$$
\begin{aligned}
|\Phi_m(t)| &\lesssim \frac{R_{ES}}{c} &\simeq 5 \times 10^2 \text{ s}, \\
|\dot{\Phi}_m(t)| &\lesssim \frac{\Omega_o R_{ES}}{c} &\simeq 1 \times 10^{-4}.
\end{aligned}
\tag{101}
$$

Assuming the maximum observation time $T_o = 120$ days to a very good approximation we have

$$T_b := t_b(T_o) \cong T_o, \quad \frac{dt}{dt_b} \cong 1. \tag{102}$$

Thus in the new time coordinate the integrals F_{1a} and F_{1b} can be very well approximated by

$$F_{1a} \cong \int_{-T_o/2}^{T_o/2} x[t(t_b)]a[t(t_b)] \exp\{-i\Phi_s[t(t_b)]\} \exp(-i2\pi f_0 t_b) \, dt_b, \tag{103}$$

$$F_{1b} \cong \int_{-T_o/2}^{T_o/2} x[t(t_b)]b[t(t_b)] \exp\{-i\Phi_s[t(t_b)]\} \exp(-i2\pi f_0 t_b) \, dt_b. \tag{104}$$

Hence we see that with the new time coordinate t_b the two integrals (103) and (104) are Fourier transforms of the functions $x[t(t_b)]a[t(t_b)] \exp\{-i\Phi_s[t(t_b)]\}$ and $x[t(t_b)]b[t(t_b)] \exp\{-i\Phi_s[t(t_b)]\}$, respectively. To calculate these integrals for a given set of phase parameters we need to perform the following numerical operations. For the chosen values of the parameters α and δ we resample the original time series according to the formula (100) and then we multiply the resampled time series $x(t_b)$ by functions $a(t_b) \exp\{-i\Phi_s[t(t_b)]\}$ and $b(t_b) \exp\{-i\Phi_s[t(t_b)]\}$. Then we calculate the two Fourier transforms (using FFT algorithm). The resampling technique has been proposed by one of us [15] and considered as an effective data analysis tool for searches of gravitational waves from periodic sources [21].

Alternatively one could define new spindown parameters

$$f_k := \frac{\overset{(k)}{f_0}}{f_0}, \quad k = 1, \ldots, s, \tag{105}$$

and introduce a different time coordinate

$$t_b'(t) = t + \Phi_m(t) + \Phi_s'(t), \tag{106}$$

where

$$\Phi_s'(t) = \sum_{k=1}^{s} f_k \frac{t^{k+1}}{(k+1)!} \tag{107}$$

and perform the resampling process according to the formula (106).

The functions a, b and consequently A, B, C, and D are known and they depend on the declination, the right ascension and the time of observation. Their values can be calculated and stored for a fine grid of positions of the neutron star on the sky and appropriate observation times before the data analysis is carried out.

The normalized reduced functional for the second component of the signal can be calculated in a similar way. Here the corresponding Fourier transforms are given by

$$F_{2a} \cong \int_{-T_o/2}^{T_o/2} x[t(t_b)]a[t(t_b)] \exp\{-i2\Phi_s[t(t_b)]\} \exp(-i4\pi f_0 t_b) \, dt_b, \tag{108}$$

$$F_{2b} \cong \int_{-T_o/2}^{T_o/2} x[t(t_b)]b[t(t_b)] \exp\{-i2\Phi_s[t(t_b)]\} \exp(-i4\pi f_0 t_b) \, dt_b. \tag{109}$$

The statistics $\mathcal{F}$ for the whole signal is then calculated from the formula

$$\mathcal{F} = \frac{4}{S_h(f_0)T_o}\frac{B|F_{1a}|^2 + A|F_{1b}|^2 - 2C\Re(F_{1a}F_{1b}^*)}{D}$$
$$+ \frac{4}{S_h(2f_0)T_o}\frac{B|F_{2a}|^2 + A|F_{2b}|^2 - 2C\Re(F_{2a}F_{2a}^*)}{D}. \tag{110}$$

The statistics $\mathcal{F}$ needs to be calculated on a multidimensional grid of parameter values (excluding the frequency parameter f_0) covering sufficiently densely the parameter space, and compared against a threshold.

4 Networks of detectors

The analysis of the previous section can be generalized to the case of a network of N interferometers in a straightforward manner. Assuming that the noise in each detector is uncorrelated with the others, the likelihood function for the network is the sum of the likelihood functions for the individual detectors. Therefore we define a statistics $\mathcal{F}_n$ for the whole network as the sum of the individual statistics of each detector given by Eq. (56). We maximize $\mathcal{F}_n$ with respect to the phase parameters to obtain their estimators. We calculate the estimators of the amplitudes from the analytic fomulae. Then we use a least-squares fit to estimate the parameters $(h_o, \theta, \psi, \iota, \Phi_0)$ from the $8N$ amplitude estimators. When the phase parameters of the signal are known each of the individual statistics $\mathcal{F}_i$ multiplied by a factor of 2 has χ^2 probability density distribution with 8 degrees of freedom when the signal is absent and noncental χ^2 distribution with noncentrality parameter d_i^2 when the signal is present. The Gaussian variables entering each statistics (normalized random variables z_i^n given by Eqs. (69)) have the same unit variance. Thus $2\mathcal{F}_n$ has the χ^2 distribution with $8N$ degrees of freedom when signal is absent and noncentral χ^2 distribution with noncentrality parameter $d_n^2 = \sum_{i=1}^{N} d_i^2$ when the signal is present. The quantity d_n can be defined as the *total signal-to-noise ratio* of the network. Probability of detection is then cacluated by Eq. (75). When the phase parameters of the signal are unknown similarly like in the one-detector case one can consider a random field which is a sum of the random fields for the individual detectors and investigate the correlation function for this random field to obtain independent number of cells N_c of the field. One can then calculate the false alarm probability for the network by means of Eq. (77).

We have studied the distribution of the network signal-to-noise ratios d_{n1}, d_{n2}, and the total network signal-to-noise ratio $d_n \cong \sqrt{d_{n1}^2 + d_{n2}^2}$ over the angles α, δ, ψ, ι, and θ with the aid of the Monte Carlo simulations for the observation time $T_o = 120$ days. We have restricted ourselves to the three detector network of the VIRGO and two initial LIGO detectors. For each case we have generated 10000 sets of angles according to the probability measure defined by the right-hand side of Eq. (87). We have assumed that the parameter d_o given by Eq. (26) is equal to 1. The results are shown in Figure 8. We have performed simulations for two gravitational wave frequencies f_0: 100 Hz and 500 Hz.

In Table 2 we have put the means and the quartiles for the Monte Carlo simulated cumulative distribution functions of the signal-to-noise ratios d_{n1}, d_{n2}, and d_n for the three detector network of the VIRGO and two initial LIGO detectors. Adding the GEO600 and TAMA300 detectors will not significantly change these signal-to-noise ratio values, but the smaller detectors can play an important role in making coincident detections by improving the confidence that the candidate events registered by larger detectors are not due to un-modelled noise.

Acknowledgments

A   The phase of the gravitational-wave signal

We assume that in the rest frame of the neutron star the time dependence of the phase of the gravitational-wave signal can be written as a power series of the form:

$$\Psi_{\mathrm{ns}}(\tau) = \Phi_0 + 2\pi \sum_{k=0}^{s} \overset{(k)}{f_{\mathrm{ns}}} \frac{\tau^{k+1}}{(k+1)!}, \tag{111}$$

where τ is the proper time in the neutron star rest frame. The assumption (111) means that the instantaneous frequency of the signal in the rest frame of the neutron star is given as

$$f_{\mathrm{ns}}(\tau) := \frac{1}{2\pi} \frac{d\Psi_{\mathrm{ns}}(\tau)}{d\tau} = \sum_{k=0}^{s} \overset{(k)}{f_{\mathrm{ns}}} \frac{\tau^k}{k!}, \tag{112}$$

so $\overset{(k)}{f_{\mathrm{ns}}}$ is the kth time derivative of the frequency evaluated at $\tau = 0$.

We assume that the neutron star is moving with respect to the SSB uniformly along a straight line according to the equation

$$\mathbf{r}_{\mathrm{ns}}(t) = r_0 \mathbf{n}_0 + v_{\mathrm{ns}} \mathbf{n}_v \left(t + \frac{r_0}{c} \right), \tag{113}$$

where $r_0 := |\mathbf{r}_{\mathrm{ns}}(t = -r_0/c)|$, $\mathbf{n}_0 := \mathbf{r}_{\mathrm{ns}}(t = -r_0/c)/r_0$. If we denote by $\mathbf{v}_{\mathrm{ns}}$ the constant velocity vector of the neutron star then $v_{\mathrm{ns}} := |\mathbf{v}_{\mathrm{ns}}|$ and $\mathbf{n}_v := \mathbf{v}_{\mathrm{ns}}/v_{\mathrm{ns}}$. The time t in Eq. (113) is the time coordinate in the SSB rest frame. We do not allow the neutron star to have an intrinsic acceleration. This means we exclude binary neutron stars, except of the binary periods so long that the acceleration effects may be accurately approximated by a Taylor series during the observation time.

The phase observed at the SSB at some time t was emitted by the star at the coordinate time t' such that

$$t = t' + \frac{|\mathbf{r}_{\mathrm{ns}}(t')|}{c}. \tag{114}$$

One can show that the relation between the time t' and the star's proper time τ is as follows

$$\tau = \sqrt{1 - \beta_{\mathrm{ns}}^2} \left(t' + \frac{r_0}{c} \right), \tag{115}$$

where $\beta_{\mathrm{ns}} := v_{\mathrm{ns}}/c$. In Eq. (115) the time dilation effect is taken into account. We have also assumed that $\tau = 0$ when the star's position vector w.r.t. the SSB is $r_0 \mathbf{n}_0$. We can now write

$$\Psi_{\mathrm{SSB}}(t) = \Psi_{\mathrm{ns}}(\tau(t)), \tag{116}$$

where $\Psi_{\mathrm{SSB}}(t)$ is the phase observed at the SSB at time t, and the time τ can be expressed in terms of t by means of Eqs. (114) and (115).

Collecting Eqs. (111) and (114)–(116) together we can write

$$\Psi_{\mathrm{SSB}}(t) = \Phi_0 + 2\pi \sum_{k=0}^{s} \frac{\overset{(k)}{f_{\mathrm{ns}}}}{(k+1)!} \left(1 - \beta_{\mathrm{ns}}^2 \right)^{(k+1)/2} \left(t'(t) + \frac{r_0}{c} \right)^{k+1}, \tag{117}$$

where t' is the solution of Eq. (114) for a given time t. It reads

$$t' = \frac{1}{1 - \beta_{\mathrm{ns}}^2} \left\{ t + \frac{r_0}{c} \beta_{\mathrm{ns}} \left[\beta_{\mathrm{ns}} + (\mathbf{n}_0 \cdot \mathbf{n}_v) \right] \right.$$
$$\left. - \sqrt{\beta_{\mathrm{ns}}^2 t^2 + 2 \frac{r_0}{c} \beta_{\mathrm{ns}} \left[\beta_{\mathrm{ns}} + (\mathbf{n}_0 \cdot \mathbf{n}_v) \right] t + \frac{r_0^2}{c^2} \left[1 + \beta_{\mathrm{ns}} (\mathbf{n}_0 \cdot \mathbf{n}_v) \right]} \right\}. \tag{118}$$

We expand the function Ψ_{SSB} given by Eqs. (117) and (118) w.r.t. time t around $t = 0$. The first few terms of the expansion read

$$\frac{\Psi_{\mathrm{SSB}}(t) - \Phi_0}{2\pi} = \overset{(0)}{f_{\mathrm{SSB}}} t + \left\{ \overset{(1)}{f_{\mathrm{SSB}}} + \frac{\left((\mathbf{n}_0 \cdot \mathbf{n}_v)^2 - 1 \right) \beta_{\mathrm{ns}}^2}{(1 + (\mathbf{n}_0 \cdot \mathbf{n}_v)\beta_{\mathrm{ns}})^2 (r_0/c)} \overset{(0)}{f_{\mathrm{SSB}}} \right\} \frac{t^2}{2}$$
$$+ \left\{ \overset{(2)}{f_{\mathrm{SSB}}} + \frac{3 \left((\mathbf{n}_0 \cdot \mathbf{n}_v)^2 - 1 \right) \beta_{\mathrm{ns}}^2}{(1 + (\mathbf{n}_0 \cdot \mathbf{n}_v)\beta_{\mathrm{ns}})^2 (r_0/c)} \left[\overset{(1)}{f_{\mathrm{SSB}}} - \frac{(\beta_{\mathrm{ns}} + (\mathbf{n}_0 \cdot \mathbf{n}_v))\beta_{\mathrm{ns}}}{(1 + (\mathbf{n}_0 \cdot \mathbf{n}_v)\beta_{\mathrm{ns}})^2 (r_0/c)} \overset{(0)}{f_{\mathrm{SSB}}} \right] \right\} \frac{t^3}{6} + \mathcal{O}(t^4), \tag{119}$$

where

$$\overset{(k)}{f}_{\text{SSB}} := \frac{\left(1 - \beta_{\text{ns}}^2\right)^{(k+1)/2}}{\left(1 + (\mathbf{n}_0 \cdot \mathbf{n}_v) \beta_{\text{ns}}\right)^{k+1}} \overset{(k)}{f}_{\text{ns}}, \quad k = 0, \dots, s. \tag{120}$$

As a result of the motion of the neutron star w.r.t. the SSB the Taylor expansion (119) of the phase Ψ_{SSB} contains infinitely many terms, even if we restrict, as in Eq. (111), the intrinsic spindown of the star to finite number of terms. When the neutron star moves radially w.r.t. the SSB then $(\mathbf{n}_0 \cdot \mathbf{n}_v)^2 = 1$ and the function Ψ_{SSB} can *exactly* be written as the finite sum:

$$\Psi_{\text{SSB}}(t) = \Phi_0 + 2\pi \sum_{k=0}^{s} \overset{(k)}{f}_{\text{SSB}} \frac{t^{k+1}}{(k+1)!}. \tag{121}$$

We shall assume the following polynomial model of the phase of the gravitational radiation observed at the SSB:

$$\Psi_{\text{SSB}}(t) = \Phi_0 + 2\pi \sum_{k=0}^{s} \overset{(k)}{f}_0 \frac{t^{k+1}}{(k+1)!}, \tag{122}$$

where the new spindown parameters $\overset{(k)}{f}_0$ do not in general coincide with the Doppler scaled intrinsic spindown parameters $\overset{(k)}{f}_{\text{SSB}}$ defined by Eq. (120).

We write the position vector $\mathbf{r}_{\text{d}}$ of the detector with respect to the SSB as

$$\mathbf{r}_{\text{d}}(t) = r_{\text{d}}(t)\mathbf{n}_{\text{d}}(t), \tag{123}$$

where $r_{\text{d}}(t) := |\mathbf{r}_{\text{d}}(t)|$ and $\mathbf{n}_{\text{d}}(t) := \mathbf{r}_{\text{d}}(t)/r_{\text{d}}(t)$. The phase of the gravitational-wave signal at the time t at the detector's location corresponds to the phase near the neutron star at an earlier instant of time t'', where t'' is the solution of the equation

$$t = t'' + \frac{|\mathbf{r}_{\text{ns}}(t'') - \mathbf{r}_{\text{d}}(t)|}{c}. \tag{124}$$

The same value of the phase is observed at the SSB at time

$$t'' + \frac{|\mathbf{r}_{\text{ns}}(t'')|}{c},$$

thus using Eq. (122) we can write

$$\Psi_{\text{d}}(t) = \Phi_0 + 2\pi \sum_{k=0}^{s} \frac{\overset{(k)}{f}_0}{(k+1)!} \left(t''(t) + \frac{|\mathbf{r}_{\text{ns}}(t''(t))|}{c} \right)^{k+1}, \tag{125}$$

where $t''(t)$ is the solution of Eq. (124) for given time t. Using Eqs. (113) and (123) we express the solution t'' to Eq. (124) in terms of the time t and the two small parameters β_{ns} and $x := r_{\text{d}}/r_0$:

$$\begin{aligned}
t''(x, \beta_{\text{ns}}) &= \frac{1}{1 - \beta_{\text{ns}}^2} \Bigg\{ t + \frac{r_0}{c} \beta_{\text{ns}} [(\mathbf{n}_0 \cdot \mathbf{n}_v) - (\mathbf{n}_{\text{d}} \cdot \mathbf{n}_v)x + \beta_{\text{ns}}] \\
&\quad - \left[\left(t + \frac{r_0}{c} \beta_{\text{ns}} [(\mathbf{n}_0 \cdot \mathbf{n}_v) - (\mathbf{n}_{\text{d}} \cdot \mathbf{n}_v)x + \beta_{\text{ns}}] \right)^2 + \left(1 - \beta_{\text{ns}}^2\right) \right. \\
&\quad \left. \times \left(\frac{r_0^2}{c^2} \left[1 + \beta_{\text{ns}}^2 - 2(\mathbf{n}_0 \cdot \mathbf{n}_{\text{d}})x + x^2 + 2 \left((\mathbf{n}_0 \cdot \mathbf{n}_v) - (\mathbf{n}_{\text{d}} \cdot \mathbf{n}_v)x \right) \beta_{\text{ns}} \right] - t^2 \right) \right]^{1/2} \Bigg\}. \tag{126}
\end{aligned}$$

Using Eq. (123) we also find that

$$\frac{|\mathbf{r}_{\text{ns}}(t'')|}{c} = \sqrt{\frac{r_0^2}{c^2} + 2\frac{r_0}{c} \left(t'' + \frac{r_0}{c} \right) (\mathbf{n}_0 \cdot \mathbf{n}_v)\beta_{\text{ns}} + \left(t'' + \frac{r_0}{c} \right)^2 \beta_{\text{ns}}^2}. \tag{127}$$

We now study how to simplify the phase Ψ_{d} given by Eqs. (125)–(127).

19

An optimal method to detect our signal in noise developed in Section 3 involves correlating the data with templates of the signal. In general if the phase of the template differs from that of the signal by as little as 1/4 of a cycle the correlation will be significantly reduced. Thus we adopt the criterion that *we exclude an effect from the model of the signal in the case when it contributes less than 1/4 of a cycle to the phase of the signal during the observation time.* That this criterion is only a sufficient condition but not necessary follows from the correlations among parameters of the phase. The shifts in the values of the parameters in the template phase away from the true values of the parameters in the signal phase can compensate for the effects in the signal not taken into account in the templates. This effect was observed for the case of coalescing binaries [34, 38, 39, 40]. Finally we stress that such shifts in the template parameter values mean that the estimators of the parameters of the signal when using an inaccurate template will be biased. It may happen that these biases are much larger than the rms errors of the estimators. Thus templates accurate to 1/4 of a cycle over the observation time may not be needed to detect the signal, but they will be needed to obtain accurate estimates of the errors in parameter measurements.

In calculating the number of cycles we assume a long observation time of 120 days, the maximum gravitational wave frequency of 1 kHz, and the extreme case of a neutron star at a distance $r_0 = 40$ pc with $v_{\mathrm{ns}} = 10^3$ km/s. For this extreme case the parameters x and β_{ns} assume the values (as to a good approximation $r_{\mathrm{d}} \cong 1$ AU):

$$x = 1.21 \times 10^{-7}, \quad \beta_{\mathrm{ns}} = 3.34 \times 10^{-3}. \tag{128}$$

The numerical values of the spindown parameters $\overset{(k)}{f_0}$ we estimate by means of the relation:

$$\left| \overset{(k)}{f_0} \right| \simeq k! \frac{f_0}{\tau^k}, \tag{129}$$

where f_0 is the radiation frequency and τ is the spindown age of the neutron star. As the extreme case we will consider $\tau = 40$ years.

It is convenient to carry out the Taylor expansion of the phase (125) with respect to the parameters x and β_{ns}. We note that for any n

$$\frac{\partial^n \Psi_{\mathrm{d}}}{\partial \beta_{\mathrm{ns}}^n} (x = 0, \beta_{\mathrm{ns}} = 0) = 0.$$

Analysis of the first few terms of the Taylor expansion shows that for the observation times $T_0 \leq 120$ days, neutron star distances $r_0 \geq 40$ pc, velocities $v_{\mathrm{ns}} \leq 10^3$ km/s, frequencies $f_0 \leq 1$ kHz, and spindown ages $\tau \geq 40$ years, the only terms which can contribute more than 1/4 of a cycle to the phase of the signal, read

$$\Psi_{\mathrm{d}} \cong \Phi_0 + 2\pi \sum_{k=0}^{4} \overset{(k)}{f_0} \frac{t^{k+1}}{(k+1)!} + \frac{2\pi}{c} \left(\mathbf{n}_0 + \frac{\mathbf{v}_{\mathrm{ns}\perp}}{r_0} t \right) \cdot \mathbf{r}_{\mathrm{d}} \sum_{k=0}^{3} \overset{(k)}{f_0} \frac{t^k}{k!}, \tag{130}$$

where $\mathbf{v}_{\mathrm{ns}\perp} := \mathbf{v}_{\mathrm{ns}} - (\mathbf{n}_0 \cdot \mathbf{v}_{\mathrm{ns}}) \mathbf{n}_0$ is the component of the velocity $\mathbf{v}_{\mathrm{ns}}$ perpendicular to the vector $\mathbf{n}_0$. The ratio $\mathbf{v}_{\mathrm{ns}\perp}/r_0$ determines the proper motion of the star. The term in the above expansion proportional to $\mathbf{v}_{\mathrm{ns}\perp}/r_0$ contributes at most ~ 4 cycles. We shall not consider it in this paper. We shall look at the possibility of its determination in the next paper of this series. Consequently we restrict ourselves to a phase model at the detector of the form

$$\Psi_{\mathrm{d}} \cong \Phi_0 + 2\pi \sum_{k=0}^{4} \overset{(k)}{f_0} \frac{t^{k+1}}{(k+1)!} + \frac{2\pi}{c} \mathbf{n}_0 \cdot \mathbf{r}_{\mathrm{d}} \sum_{k=0}^{3} \overset{(k)}{f_0} \frac{t^k}{k!}. \tag{131}$$

The model (131) contains the position $\mathbf{r}_{\mathrm{d}}$ of the Earth relative to the SSB, which we now consider. In addition we must consider extra, purely relativistic effects left out of (131).

Motion of the Earth w.r.t. the SSB is very well determined and there are several computer ephemeris routines available [20]. In this paper we assume for simplicity that the Earth moves on a circular orbit around the Sun. The eccentricity of the Earth's orbit ($e_{\oplus} = 0.017$) introduces a change of about 8.3×10^3 cycles in the phase w.r.t. the phase for circular orbit for 1 kHz signal, so it must be included in realistic filters. But it introduces no new parameters so we ignore it here. We also ignore the motion of the Earth around the Earth-Moon barycenter.

There are two types of relativistic corrections. One originates in the difference between the coordinate time t which we used in the derivation of the phase model and the proper time τ in the detector's reference frame. The difference is due to the combined effect of the gravitational redshift and the time dilation. The other correction is the Shapiro delay caused by propagation of the gravitational wave through the curved spacetime of the solar system. We estimate the contribution to the number of cylces in the phase produced by these corrections.

The difference between the coordinate time t in the first order post-Newtonian coordinate system which is assumed to be the rest frame of the SSB and the proper time τ kept by a terrestial clock is discussed in detail in Ref. [41]. The difference $\Delta_E := t - \tau$ is given by the integral

$$\Delta_E = \frac{1}{c^2} \int_0^t \left\{ U\left[\mathbf{r}(t')\right] + \frac{v(t')^2}{2} \right\} dt', \tag{132}$$

where $\mathbf{r}$ is the position vector of the clock w.r.t. the SSB, $\mathbf{v} := \dot{\mathbf{r}}$ is the clock's coordinate velocity, and $U\left[\mathbf{r}(t)\right]$ is the instantaneous gravitational potential at the clock's location. The time difference described by the integral (132) can be split into the secular and periodic part. The secular difference is due to the practically constant rotational velocity and the Earth's gravitational potential at the detector's location as well as the average orbital velocity of the Earth and the average gravitational potential along the Earth's orbit. This secular difference corresponds to the rescaling of the time coordinate and can be incorporated into the definition of the spindown parameters. The main contribution to the periodic part of the integral (132) was calculated by Clemence and Szebehely [42] and then corrected by Blandford and Teukolsky [43]. It can be written as

$$(\Delta_E)_{\text{periodic}} \cong \frac{2GM_\odot e_\oplus}{c^2 a_\oplus \left(1 - e_\oplus^2\right) \Omega_o} \left[\left(1 - \frac{1}{8}e_\oplus^2\right) \sin M_\oplus + \frac{1}{2}e_\oplus \sin 2M_\oplus + \frac{3}{8}e_\oplus^2 \sin 3M_\oplus \right], \tag{133}$$

where $M_\odot$ is the mass of the Sun, $a_\oplus = 1$ AU, Ω_o is the mean orbital angular velocity of the Earth, $e_\oplus$ and $M_\oplus$ are the eccentricity and mean anomaly of the Earth's orbit. The quantity $(\Delta_E)_{\text{periodic}}$ varies in time with the period of one year and has the amplitude $\simeq 1.7 \times 10^{-3}$ s, so for a 1 kHz gravitational wave the contribution of this correction to the total number of cycles is not greater than ~ 2 cycles. Even when it must be included in a filter, it introduces no new parameters.

The magnitude of the Shapiro delay can be estimated from the relation [44] (neglecting the eccentricity of the Earth's orbit)

$$\Delta_S = \frac{2GM_\odot}{c^3} \log \frac{1}{1 + \cos\theta}, \tag{134}$$

where θ is the star-Sun-detector angle at the time of observation. To estimate the maximum value of the Shapiro delay we consider a neutron star in such position that at some instant of time the line of sight from the detector to the neutron star is tangent to the surface of the Sun. Then $\theta = \theta_1 \simeq \pi - \zeta$, where $\zeta \simeq R_\odot/1$ AU $\simeq 4.65 \times 10^{-3}$ rad ($R_\odot$ is the radius of the Sun). Six months later $\theta = \theta_2 \simeq \zeta$, so the amplitude of the correction is

$$\Delta_S\left(\theta = \theta_1\right) - \Delta_S\left(\theta = \theta_2\right) \simeq \frac{2GM_\odot}{c^3} \log \frac{1 + \cos\theta_2}{1 + \cos\theta_1} \simeq 1.2 \times 10^{-4} \text{ s}.$$

For a 1 kHz gravitational wave this gives ~ 0.1 cycles. So the Shapiro delay will be unobservable.

We see that the relativistic corrections that need to be applied to our formula are small. By our $1/4$ of a cycle criterion they can be neglected if we search for signals with frequencies less than ~ 100 Hz. We shall not consider these corrections in this and the following papers of the series since they are unlikely influence our results. However they may need to be included in filters.

B Signal-to-noise ratio

In this appendix we give the detailed expressions for the functions A_1, A_2, B_1, and B_2 from Eqs. (85) and (86). They read:

$$A_k\left(\delta, \psi, \iota\right) = F_k(\iota)e_1(\delta)\cos 4\psi + G_k(\iota)e_2(\delta), \tag{135}$$

$$B_k\left(\alpha, \delta, \psi, \iota; T_o\right) = \frac{1}{\Omega_r} \sum_{n=1}^{4} \sin\left(n\frac{\Omega_r}{2}T_o\right)$$
$$\times \left\{ C_{kn}\left(\delta, \psi, \iota\right) \cos\left[n(\alpha - \phi_r)\right] + D_{kn}\left(\delta, \psi, \iota\right) \sin\left[n(\alpha - \phi_r)\right] \right\}, \quad (136)$$

where Ω_r is the rotational frequency of the Earth, T_o is the observation time, and where

$$C_{kn}\left(\delta, \psi, \iota\right) = F_k(\iota)\left[f_{1n}(\delta)\cos 4\psi + g_{1n}(\delta)\sin 4\psi\right] + G_k(\iota)h_{1n}(\delta), \quad (137)$$

$$D_{kn}\left(\delta, \psi, \iota\right) = F_k(\iota)\left[f_{2n}(\delta)\cos 4\psi + g_{2n}(\delta)\sin 4\psi\right] + G_k(\iota)h_{2n}(\delta), \quad (138)$$

$$F_1(\iota) = -\frac{1}{16}\sin^4\iota, \quad F_2(\iota) = \frac{1}{4}\sin^4\iota, \quad (139)$$

$$G_1(\iota) = \frac{1}{16}\sin^2\iota\left(1 + \cos^2\iota\right), \quad G_2(\iota) = \frac{1}{4}\left(1 + 6\cos^2\iota + \cos^4\iota\right). \quad (140)$$

The functions e_1, e_2, f_{kn}, and g_{kn} $(k = 1, 2, n = 1, \ldots, 4)$ entering Eqs. (135), (137), and (138) are equal to

$$
\begin{aligned}
e_1(\delta) &= 4j_1\cos^4\delta, & e_2(\delta) &= 4j_2 - j_3\cos 2\delta + j_1\cos^2 2\delta, \\
f_{11}(\delta) &= -4j_4\cos^3\delta\sin\delta, & f_{12}(\delta) &= j_5\cos^2\delta\left(3 - \cos 2\delta\right), \\
f_{13}(\delta) &= -j_6\left(7 - \cos 2\delta\right)\sin 2\delta, & f_{14}(\delta) &= -j_7\left(35 - 28\cos 2\delta + \cos 4\delta\right), \\
f_{21}(\delta) &= -28j_8\cos^3\delta\sin\delta, & f_{22}(\delta) &= -7j_9\left(3 - \cos 2\delta\right)\cos^2\delta, \\
f_{23}(\delta) &= -j_{10}\left(7 - \cos 2\delta\right)\sin 2\delta, & f_{24}(\delta) &= -j_{11}\left(35 - 28\cos 2\delta + \cos 4\delta\right), \\
g_{11}(\delta) &= 28j_8\cos^3\delta, & g_{12}(\delta) &= 28j_9\cos^2\delta\sin\delta, \\
g_{13}(\delta) &= 2j_{10}\left(5 - 3\cos 2\delta\right)\cos\delta, & g_{14}(\delta) &= 16j_{11}\left(3 - \cos 2\delta\right)\sin\delta, \\
g_{21}(\delta) &= -4j_4\cos^3\delta, & g_{22}(\delta) &= 4j_5\cos^2\delta\sin\delta, \\
g_{23}(\delta) &= -2j_6\left(5 - 3\cos 2\delta\right)\cos\delta, & g_{24}(\delta) &= -16j_7\left(3 - \cos 2\delta\right)\sin\delta, \\
h_{11}(\delta) &= \left(j_{12} - j_4\cos 2\delta\right)\sin 2\delta, & h_{12}(\delta) &= \left(j_{13} - j_5\cos 2\delta\right)\cos^2\delta, \\
h_{13}(\delta) &= 4j_6\cos^3\delta\sin\delta, & h_{14}(\delta) &= -8j_7\cos^4\delta, \\
h_{21}(\delta) &= j_8\left(1 - 7\cos 2\delta\right)\sin 2\delta, & h_{22}(\delta) &= -j_9\left(5 - 7\cos 2\delta\right)\cos^2\delta, \\
h_{23}(\delta) &= 4j_{10}\cos^3\delta\sin\delta, & h_{24}(\delta) &= -8j_{11}\cos^4\delta,
\end{aligned}
$$

where the coefficients $j_1, \ldots, j_{13}$ depend on the angles λ and γ:

$$j_1\left(\lambda, \gamma\right) = \frac{1}{256}\left(4 - 20\cos^2\lambda + 35\sin^2 2\gamma\cos^4\lambda\right),$$

$$j_2\left(\lambda, \gamma\right) = \frac{1}{1024}\left(68 - 20\cos^2\lambda - 13\sin^2 2\gamma\cos^4\lambda\right),$$

$$j_3\left(\lambda, \gamma\right) = \frac{1}{128}\left(28 - 44\cos^2\lambda + 5\sin^2 2\gamma\cos^4\lambda\right),$$

$$j_4\left(\lambda, \gamma\right) = \frac{1}{32}\left(2 - 7\sin^2 2\gamma\cos^2\lambda\right)\sin 2\lambda,$$

$$j_5\left(\lambda, \gamma\right) = \frac{1}{32}\left(3 - 7\cos 4\gamma - 7\sin^2 2\gamma\cos^2\lambda\right)\cos^2\lambda,$$

$$j_6\left(\lambda, \gamma\right) = \frac{1}{96}\left(2\cos 4\gamma + \sin^2 2\gamma\cos^2\lambda\right)\sin 2\lambda,$$

$$j_7\left(\lambda, \gamma\right) = \frac{1}{1024}\left(4\cos 4\gamma\sin^2\lambda - \sin^2 2\gamma\cos^4\lambda\right),$$

$$j_8\left(\lambda, \gamma\right) = \frac{1}{32}\sin 4\gamma\cos^3\lambda,$$

$$j_9\left(\lambda, \gamma\right) = \frac{1}{32}\sin 4\gamma\cos^2\lambda\sin\lambda,$$

$$j_{10}\left(\lambda, \gamma\right) = \frac{1}{192}\sin 4\gamma\left(5 - 3\cos 2\lambda\right)\cos\lambda,$$

$$j_{11}\left(\lambda, \gamma\right) = \frac{1}{1024}\sin 4\gamma\left(3 - \cos 2\lambda\right)\sin\lambda,$$

$$j_{12}\left(\lambda, \gamma\right) = \frac{1}{32}\left(14 - \sin^2 2\gamma\cos^2\lambda\right)\sin 2\lambda,$$

$$j_{13}\left(\lambda, \gamma\right) = \frac{1}{32}\left(9 - 5\cos 4\gamma - 5\sin^2 2\gamma\cos^2\lambda\right)\cos^2\lambda.$$

C Monte Carlo analysis of the two signal-to-noise ratio components

We have also studied the distribution of the individual signal-to-noise ratios d_1^2 and d_2^2 given by Eqs. (85) and (86) over the angles α, δ, ψ, and ι by means of the Monte Carlo simulations (for the observation time $T_o = 120$ days). The results are shown in Figures 9–13. The signal-to-noise ratios d_1^2 and d_2^2 are normalized here by means of the quantities

$$\langle d_{1(120\text{days})}^2 \rangle := \langle d_1^2 \rangle_{\alpha,\delta,\psi,\iota}|_{T_o=120\text{days}}, \quad \langle d_{2(120\text{days})}^2 \rangle := \langle d_2^2 \rangle_{\alpha,\delta,\psi,\iota}|_{T_o=120\text{days}}.$$

In Tables 3 and 4 we summarize the statistical characteristics of the simulated distributions of the normalized signal-to-noise ratios d_1^2 and d_2^2. We give extremal values, means, standard deviations (std), and medians.

detector	min	max	mean	std	median
GEO600	0.0	2.0	1.0	0.45	0.96
LIGO Hanford	0.0	1.7	1.0	0.41	1.0
LIGO Livingston	0.0	1.5	1.0	0.34	1.1
VIRGO	0.0	1.6	1.0	0.36	1.1
TAMA300	0.0	1.9	1.0	0.38	1.0

Table 3: Statistics of $d_1^2/\langle d_{1(120\text{days})}^2 \rangle$.

detector	min	max	mean	std	median
GEO600	0.18	4.0	1.0	0.72	0.77
LIGO Hanford	0.12	3.3	1.0	0.68	0.79
LIGO Livingston	0.27	2.7	1.0	0.64	0.80
VIRGO	0.26	3.2	1.0	0.66	0.79
TAMA300	0.18	2.8	1.0	0.64	0.80

Table 4: Statistics of $d_2^2/\langle d_{2(120\text{days})}^2 \rangle$.

References

[1] B. F. Schutz, in *Proceedings of the September 1996 SIGRAV Meeting* (World Scientific, Singapore, 1997).

[2] K. S. Thorne, in *Three Hundred Years of Gravitation*, edited by S. W. Hawking and W. Israel (Cambridge University Press, Cambridge, 1987), Section 9.4.2(b), pp. 386–391.

[3] K. Danzmann *et al.*, in *Gravitational Wave Experiments*, edited by E. Coccia, G. Pizzella, and F. Ronga (World Scientific, Singapore, 1995), pp. 100–111.

[4] A. Abramovici *et al.*, Science **256**, 325 (1992).

[5] C. Bradaschia *et al.*, Nucl. Instrum. Methods Phys. Res. A **289**, 518 (1990).

[6] K. Tsubono *et al.*, in *Gravitational Wave Detection. Proceedings of the TAMA International Workshop on Gravitational Wave Detection*, edited by K. Tsubono, M.-K. Fujimoto, and K. Kuroda (Universal Academy Press, Tokyo, 1997), pp. 183–191.

[7] V. R. Pandharipande, D. Pines, and R. A. Smith, Astrophys. J. **208**, 550 (1976).

[8] S. Bonazzola and E. Gourgoulhon, Astron. Astr. **312**, 675 (1996).

[9] M. Zimmermann and E. Szedenits, Phys. Rev. D **20**, 351 (1979).

[10] M. Zimmermann, Phys. Rev. D **21**, 891 (1980).

[11] R. V. Wagoner, Astrophys. J. **278**, 345 (1984).

[12] B. F. Schutz, in *Mathematics of Gravitation. Part II: Gravitational Wave Detection*, edited by A. Królak (Banach Center Publications Vol. 41 Part II, Warsaw, 1997), pp. 11–17.

[13] S. Chandrasekhar, Phys. Rev. Lett. **24**, 611 (1970).

[14] J. L. Friedman and B. F. Schutz, Astrophys. J. **222**, 281 (1978).

[15] B. F. Schutz, in *The Detection of Gravitational Waves*, edited by D. G. Blair (Cambridge University Press, Cambridge, 1991), pp. 406–452.

[16] N. Andersson, A new class of unstable modes of rotating relativistic stars, preprint gr-qc/9706075, 1997.

[17] L. Lindblom, in *Relativistic Astrophysics*, edited by H. Riffert *et al.* (Vieweg Verlag, Wiesbaden, 1997).

[18] J. C. Livas, Ph. D. thesis, Massachusetts Institute of Technology, 1987.

[19] T. M. Niebauer *et al.*, Phys. Rev. D **47**, 3106 (1993).

[20] G. S. Jones, Ph. D. thesis, University of Wales, 1995.

[21] P. R. Brady, T. Creighton, C. Cutler, and B. F. Schutz, Phys. Rev. D **57**, 2101 (1998).

[22] A. Królak, in *Very High Energy Phenomena in the Universe. Proceedings of the XXXIInd Rencontres de Moriond*, edited by Y. Giraud-Héraud and J. Trân Thanh Vân (Editions Frontieres, Paris, 1997), pp. 329–334.

[23] B. F. Schutz and M. Tinto, Mon. Not. R. Astron. Soc. **224**, 131 (1987).

[24] P. Jaranowski and A. Królak, Phys. Rev. D **48**, 1723 (1994).

[25] B. Allen, Gravitational wave detector sites, gr-qc 9607075.

[26] K. Jotania and S. V. Dhurandhar, Bull. Astr. Soc. India **22**, 303 (1994).

[27] Our functions a and b from Eqs. (12) and (13) are connected with the functions S_+ and $S_\times$ from Eqs. (9) and (10) of [19] by relations: $S_+ = -4a$, $S_\times = 4b$, provided the following identification of our variables $\alpha, \delta, \lambda, \phi_r, \gamma$ with the variables $\alpha, \beta, \theta, \psi, \lambda$ used in [19] is made (assuming $\zeta = \pi/2$): $\alpha \to \beta$, $\delta \to \pi/2 - \alpha$, $\phi_r \to \lambda$, $\lambda \to \pi/2 - \theta$, $\gamma \to \psi - 5\pi/4$. The last identification means that the angle ψ is measured clockwise from the first inteferometer's arm to North.

[28] J. C. Livas, in *Gravitational Wave Data Analysis*, edited by B. F. Schutz (Kluwer, Dordrecht, 1989), pp. 217–238.

[29] B. J. Owen, Phys. Rev. D **53**, 6749 (1996).

[30] S. V. Dhurandhar and B. F. Schutz, Phys. Rev. D **50**, 2390 (1994).

[31] M. H. A. Davis, in *Gravitational Wave Data Analysis*, edited by B. F. Schutz (Kluwer, Dordrecht, 1989), pp. 73–94.

[32] C. W. Helström, *Statistical Theory of Signal Detection*, 2nd ed. (Pergamon Press, London, 1968), Sections 2(c), 2(d), and 3 of Chapter IX.

[33] D. Nicholson and A. Vecchio, Bayesian Bounds on Parameter Estimation Accuracy for Compact Coalescing Binary Gravitational Wave Signal, preprint gr-qc/9705064, 1997.

[34] C. Cutler *et al.*, Phys. Rev. Lett. **70**, 2984 (1993).

[35] B. F. Schutz, Class. Quantum Grav. **13**, A219 (1996).

[36] S. Kawamura (private communication).

[37] K. Strain (private communication).

[38] R. Balasubramanian and S. V. Dhurandhar, Phys. Rev. D **50**, 6080 (1994).

[39] B. S. Sathyaprakash, Phys. Rev. D **50**, R7111 (1994).

[40] A. Królak, in *Proceedings of the Cornelius Lanczos International Centenary Conference*, edited by J. D. Brown, M. T. Chu, D. C. Ellison, and R. J. Plemmons (SIAM, Philadelphia, 1994), p. 482.

[41] D. C. Backer and R. W. Hellings, Ann. Rev. Astron. Astrophys. **24**, 537 (1986).

[42] G. M. Clemence and V. Szebehely, Astron. J. **72**, 1324 (1967).

[43] R. Blandford and S. A. Teukolsky, Astrophys. J. **205**, 580 (1976).

[44] I. I. Shapiro, Phys. Rev. Lett. **13**, 789 (1964).
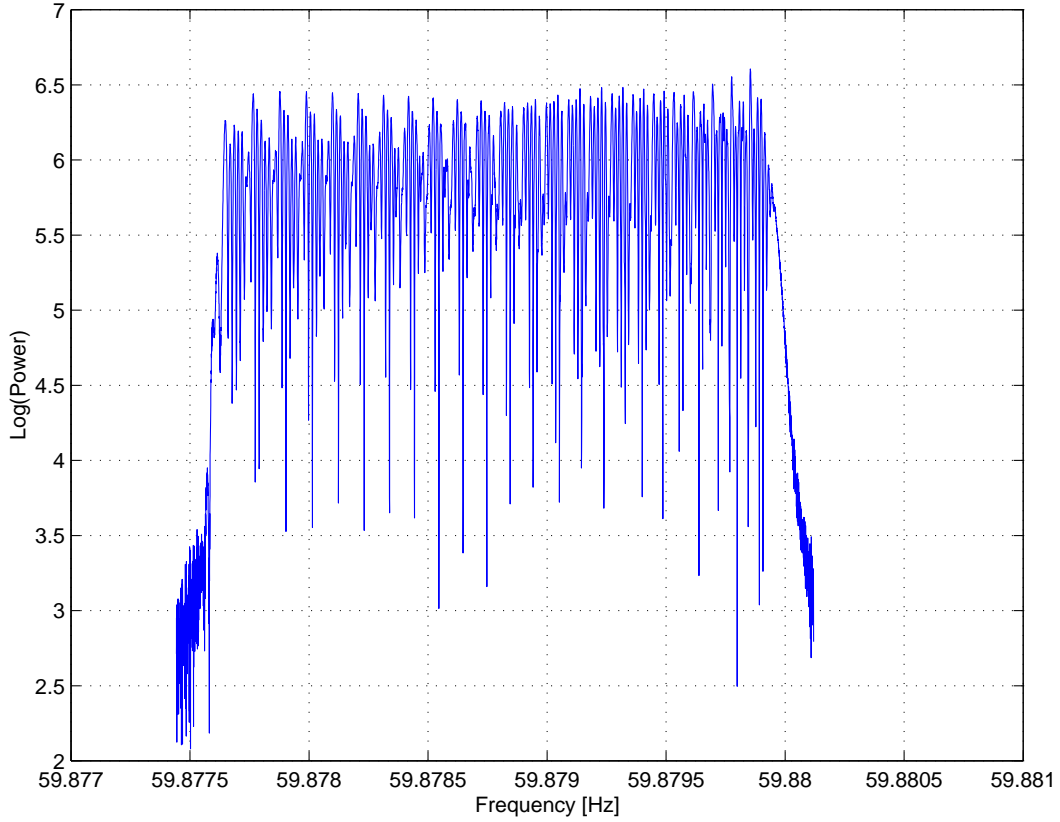
Figure 1: Power spectrum of the noise-free response of an interferometer located near Hannover to gravitational-wave signal from the Crab pulsar at twice the rotation frequency. We have assumed the frequency $f_0 = 29.937$ Hz and the spindown parameters $\overset{(1)}{f_0} = -3.773 \times 10^{-10}$ s^{-2}, $\overset{(2)}{f_0} = 0.976 \times 10^{-20}$ s^{-3}, $\overset{(3)}{f_0} = -0.615 \times 10^{-30}$ s^{-4}. A 24-day long signal was analysed corresponding to the frequency resolution of around 4.8×10^{-7} Hz. The power spectrum shows 24 main peaks resulting from the periodic phase modulation of the signal. In each interval between the main peaks there are additional subsidiary peaks arising from the amplitude modulation of the signal.
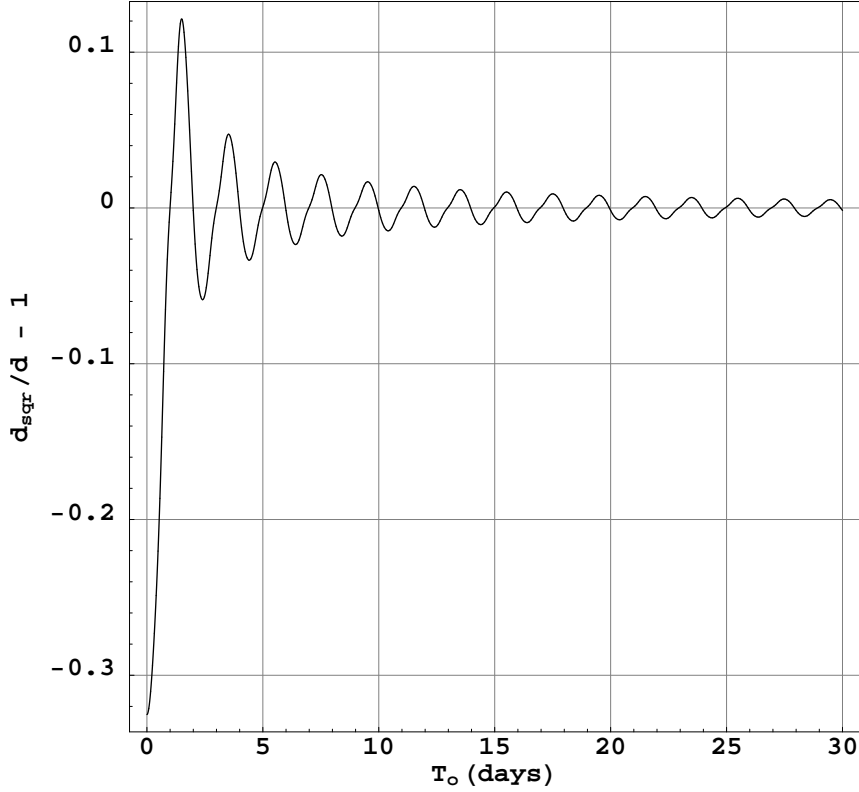
Figure 2: The relative contribution of the part d_sqr of the signal-to-noise ratio proportional to the square root of the observation time T_o to the total signal-to-noise ratio d for the GEO600 detector with the wideband noise curve ($d_\text{sqr} \approx h_o \sin\zeta [A_1 \sin^2 2\theta/S_h(f_0) + A_2 \sin^4\theta/S_h(2f_0)]^{1/2}\sqrt{T_o}$, cf. Eqs. (80), (85), and (86)). A hypothetical neutron star is assumed to be in the distance of 40 pc from the Earth and to emit gravitational waves with frequency $f_0 = 100$ Hz, star's ellipticity is 10^{-5}, its moment of inertia w.r.t. the rotation axis is 10^{45} g cm^2. We also set $\alpha - \phi_r = 15°$, $\delta = 35°$, $\psi = 11.25°$, $\iota = 22.5°$, and $\theta = 45°$.
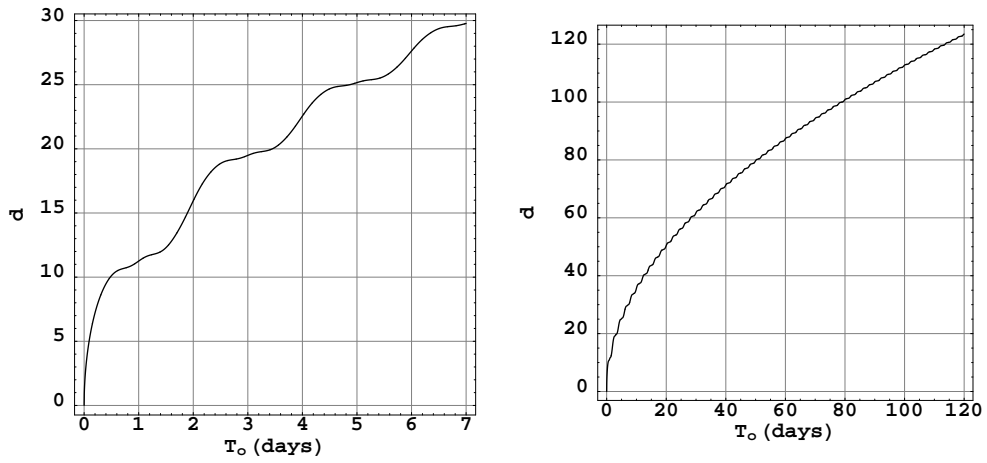
Figure 3: The total signal-to-noise ratio d as a function of the observation time T_o for the GEO600 detector (with the wideband noise curve). The neutron star parameters are the same as in Figure 2.
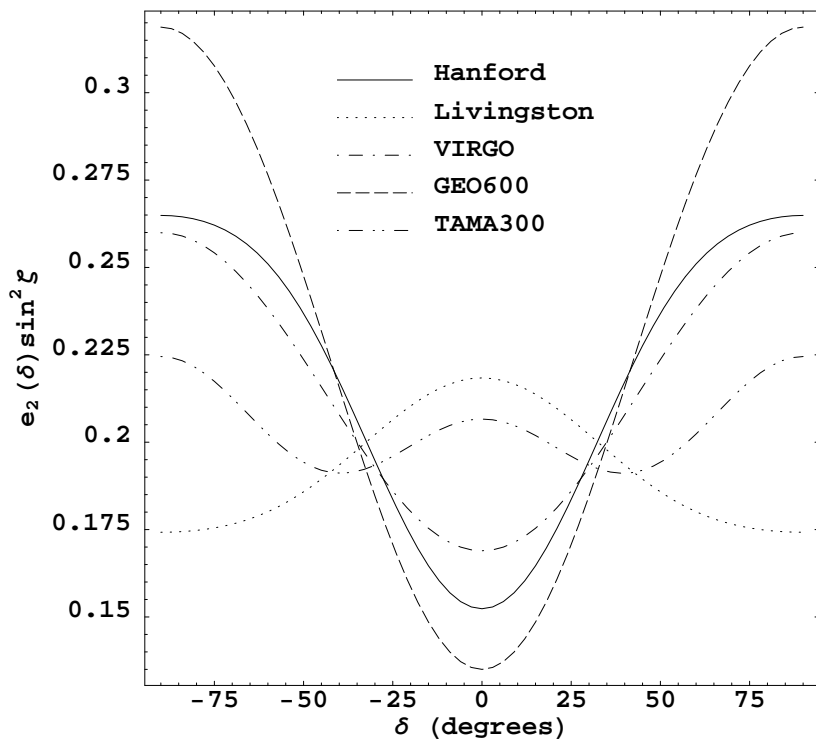
Figure 4: The plot of the product $e_2(\delta)\sin^2\zeta$ against the declination δ of the gravitational-wave source for different detectors. It can be shown (cf. Appendix B) that for a hypothetical detector located at the latitude $\lambda = \pm\arccos\sqrt{2/3} \approx \pm 35.26°$ there exist eight different orientations γ of its arms such that the function $e_2 = 1/5$, i.e. e_2 does not depend on the declination δ of the gravitational-wave source. These orientation angles are: γ_o, $90° \pm \gamma_o$, $180° \pm \gamma_o$, $270° \pm \gamma_o$, $360° - \gamma_o$, where $\gamma_o = \frac{1}{2}\arcsin\sqrt{3/5} \approx 25.38°$.
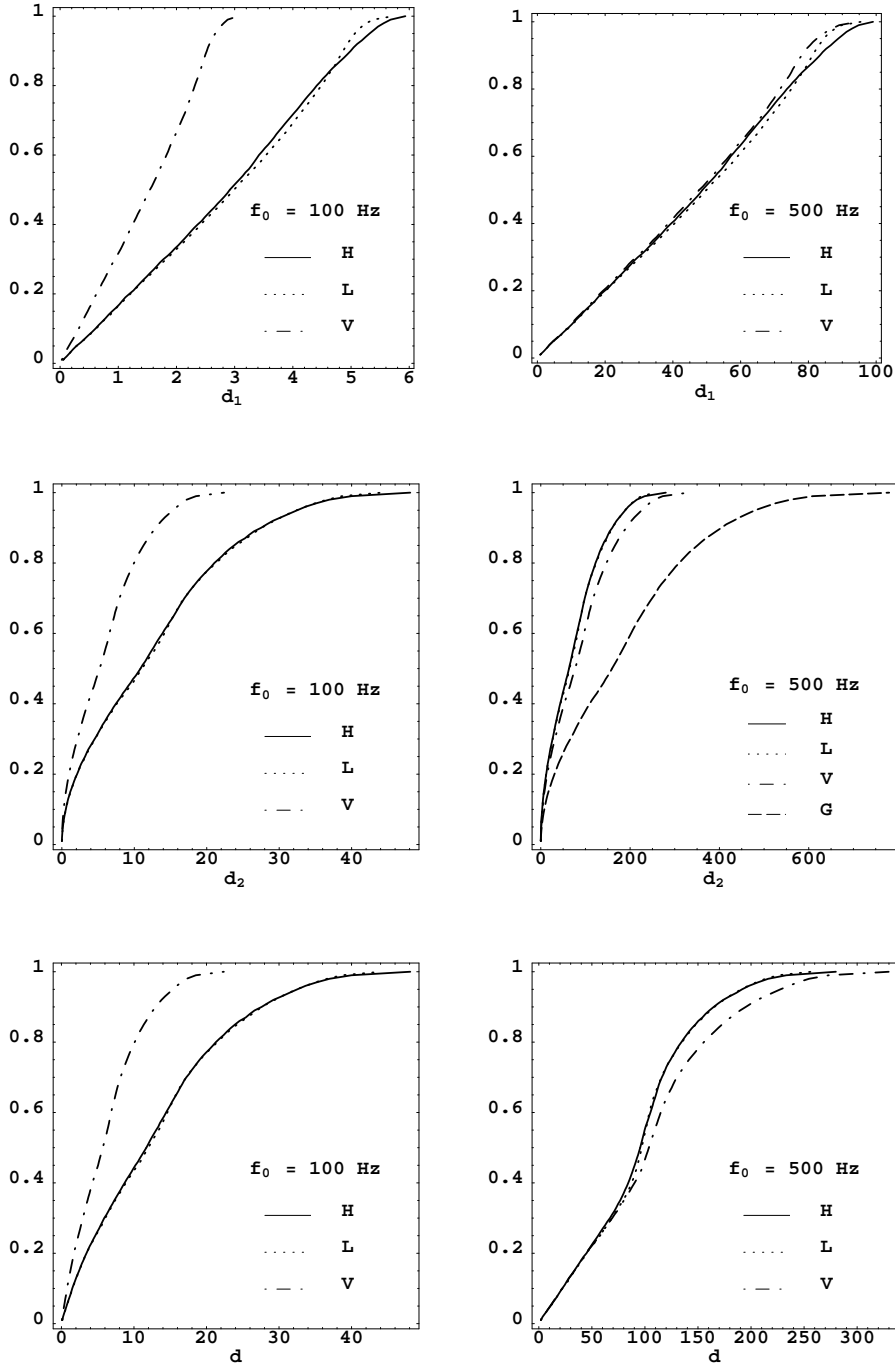
Figure 5: Cumulative distribution functions of the simulated signal-to-noise ratios d_1, d_2, and d for the VIRGO (V), initial Hanford (H), and initial Livingston (L) detectors. We assume that star's ellipticity is 10^{-5}, its moment of inertia w.r.t. the rotation axis is 10^{45} g cm^2 and its distance from the Earth is 1 kpc. The observation time is 120 days. The left column is for $f_0 = 100$ Hz and the right one is for $f_0 = 500$ Hz. We have also shown the cumulative distribution function of the signal-to-noise ratio d_2 for the GEO600 (G) detector with the narrowband noise tuned to 1 kHz with the bandwidth of 30 Hz.
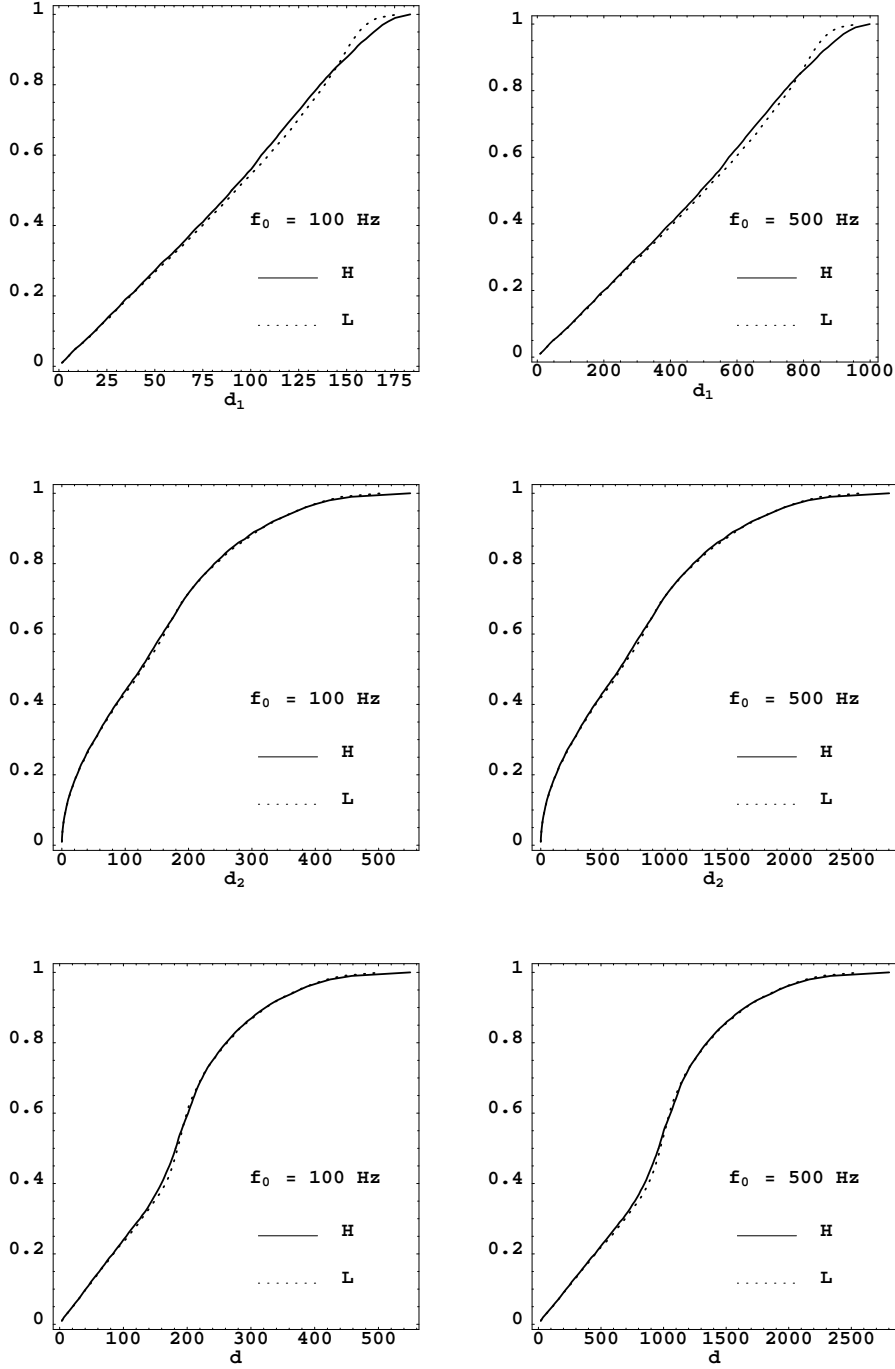
Figure 6: Cumulative distribution functions of the simulated signal-to-noise ratios d_1, d_2, and d for the advanced Hanford (H) and advanced Livingston (L) detectors. The observation time is 120 days. The left column is for $f_0 = 100$ Hz and the right one is for $f_0 = 500$ Hz. The neutron star parameters are the same as in Figure 5.
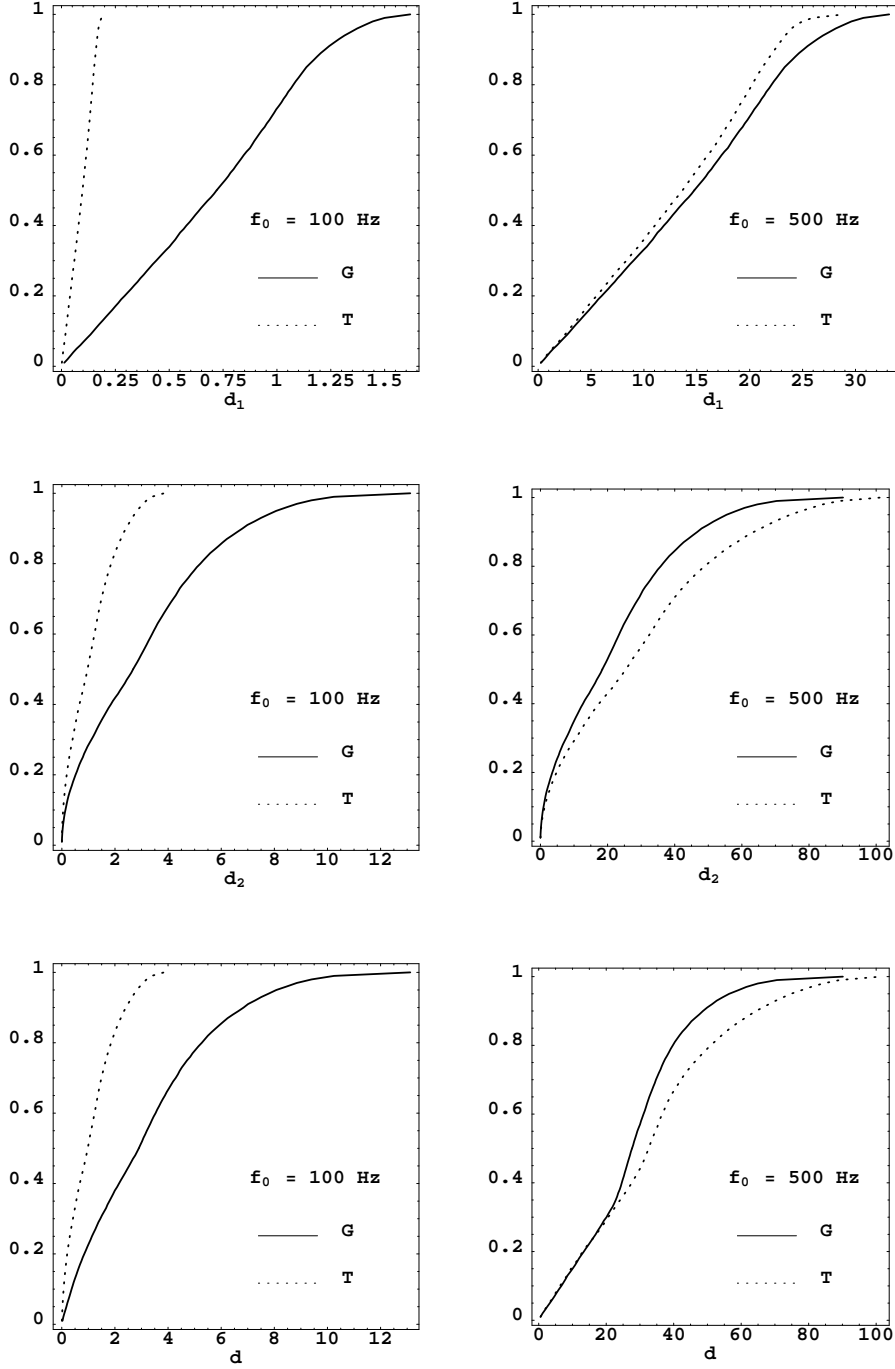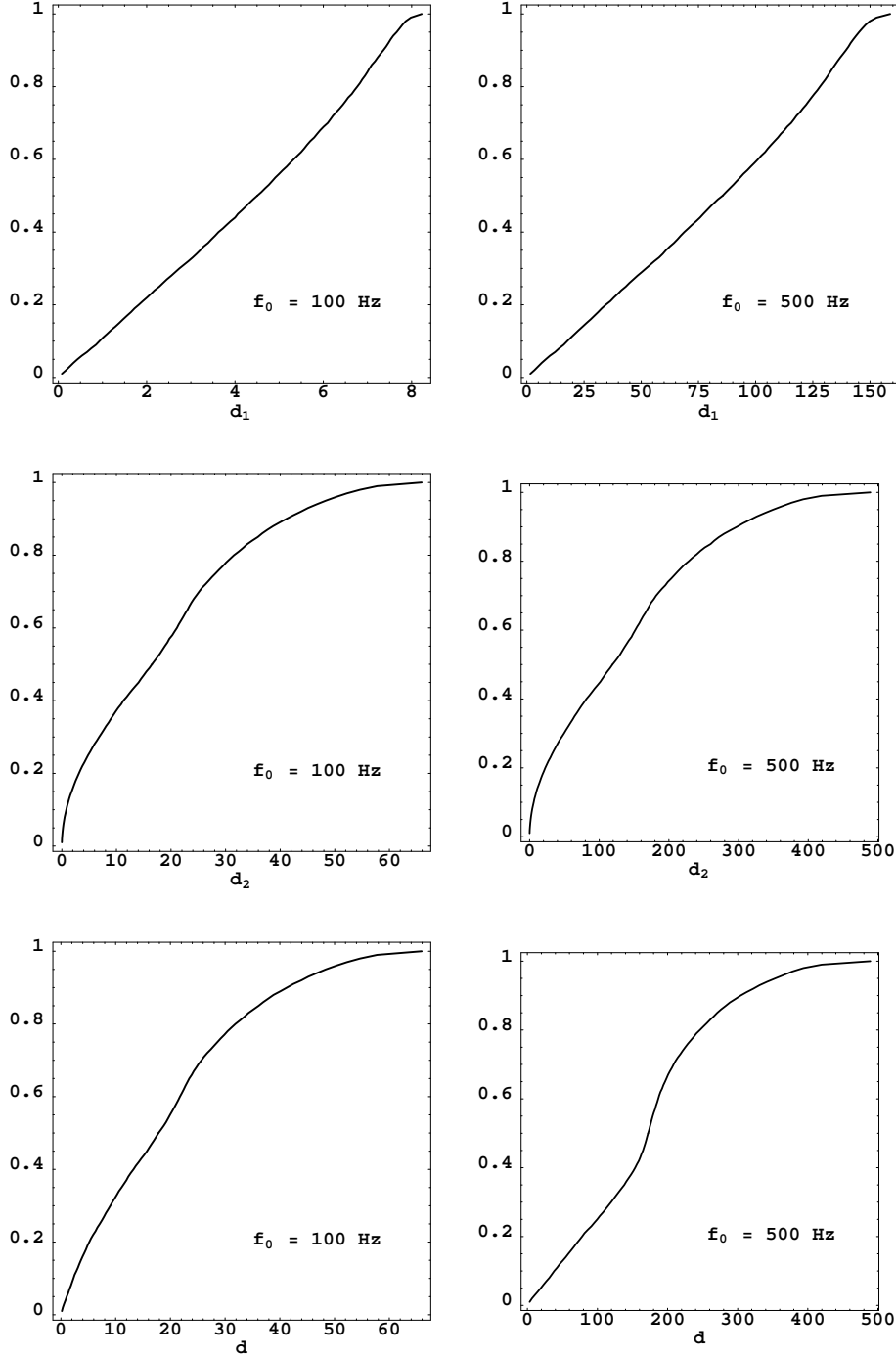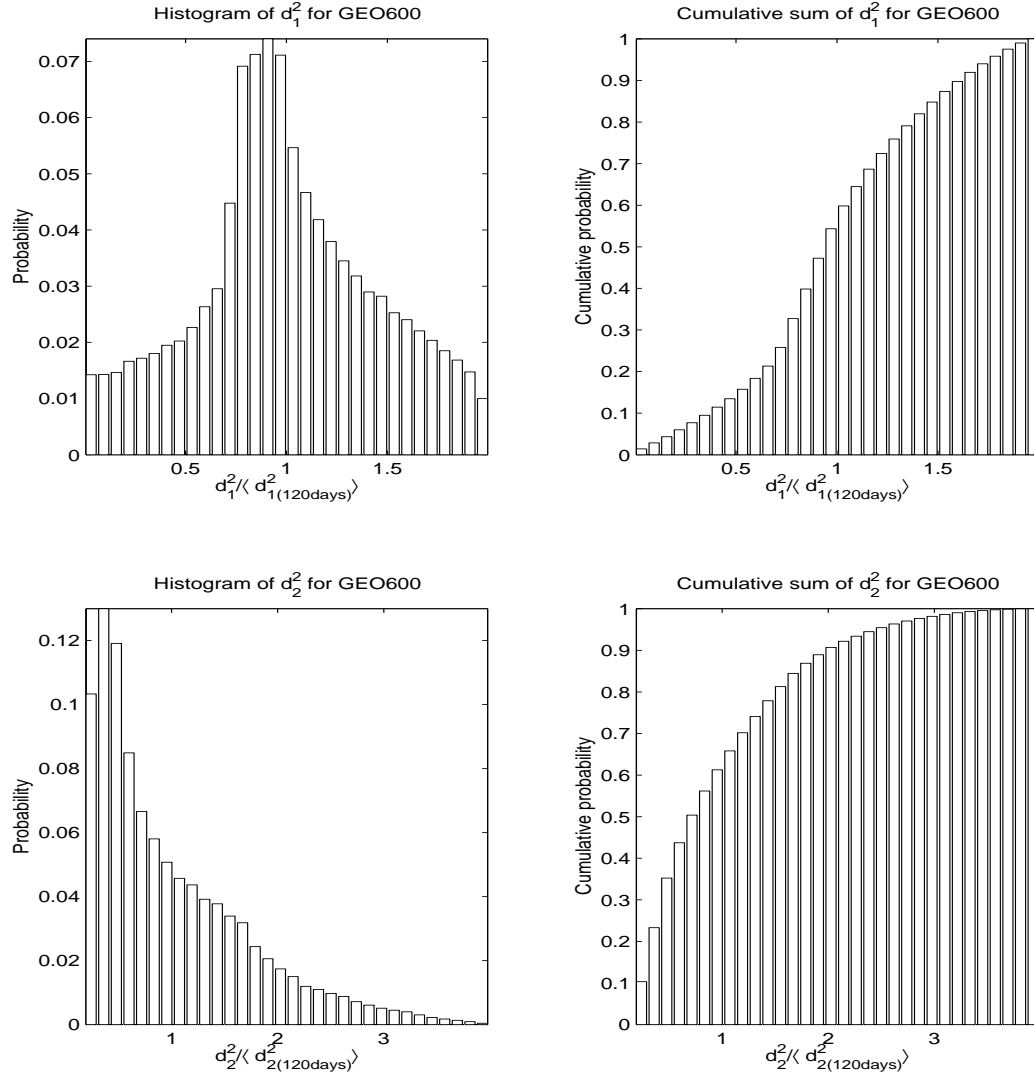
Figure 7: Cumulative distribution functions of the simulated signal-to-noise ratios d_1, d_2, and d for the GEO600 (G) with the wideband noise curve and TAMA300 (T) detectors. The observation time is 120 days. The left column is for $f_0 = 100$ Hz and the right one is for $f_0 = 500$ Hz. The neutron star parameters are the same as in Figure 5.

Figure 8: Cumulative distribution functions of the simulated signal-to-noise ratios d_{n1}, d_{n2}, and d_n for the three detector network of the VIRGO and two initial LIGO detectors. The observation time is 120 days. The left column is for $f_0 = 100$ Hz and the right one is for $f_0 = 500$ Hz. The neutron star parameters are the same as in Figure 5.
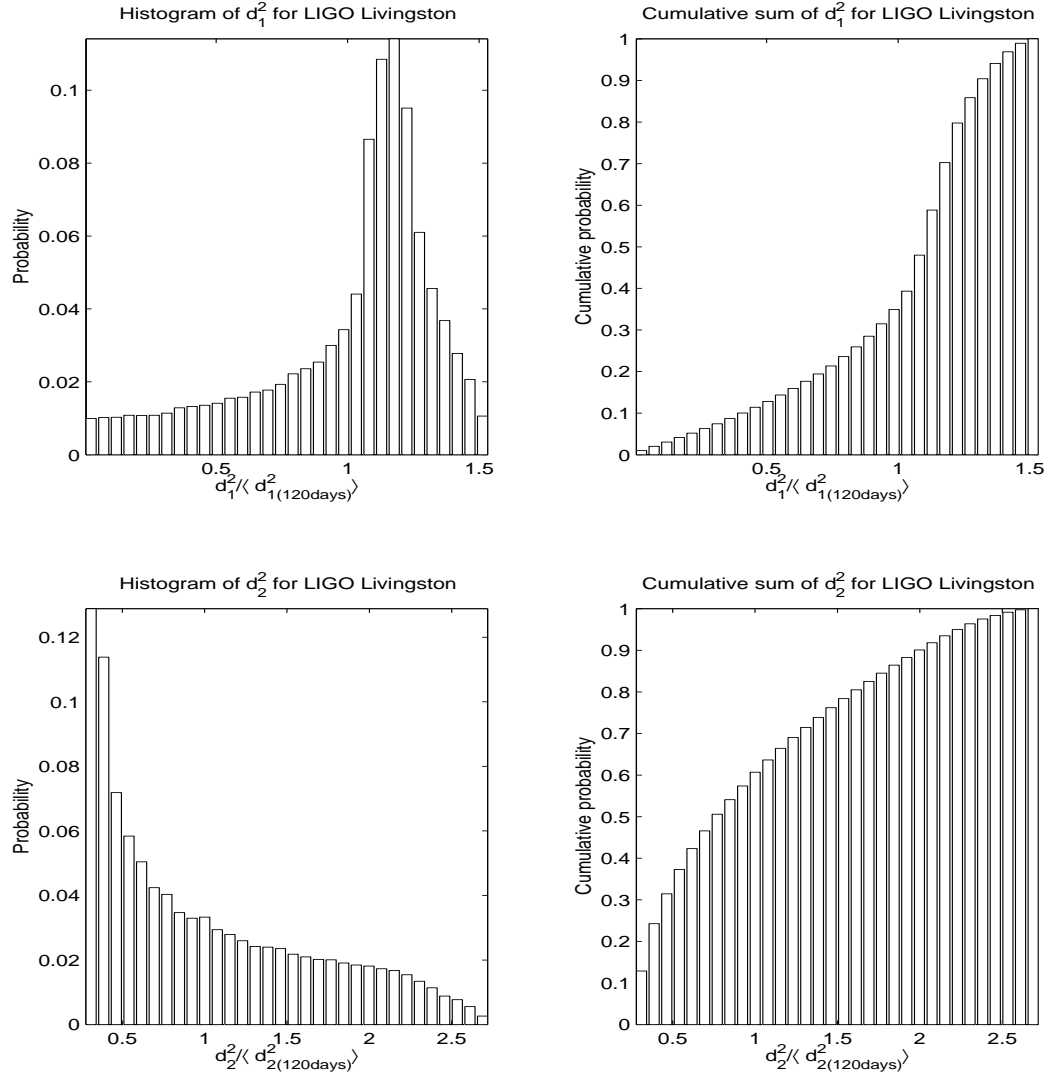
Figure 9: Histograms of the simulated probability density and cumulative distribution functions of the normalized signal-to-noise ratios $d_1^2/\langle d_{1(120\mathrm{days})}^2\rangle$ and $d_2^2/\langle d_{2(120\mathrm{days})}^2\rangle$ for the GEO600 detector.
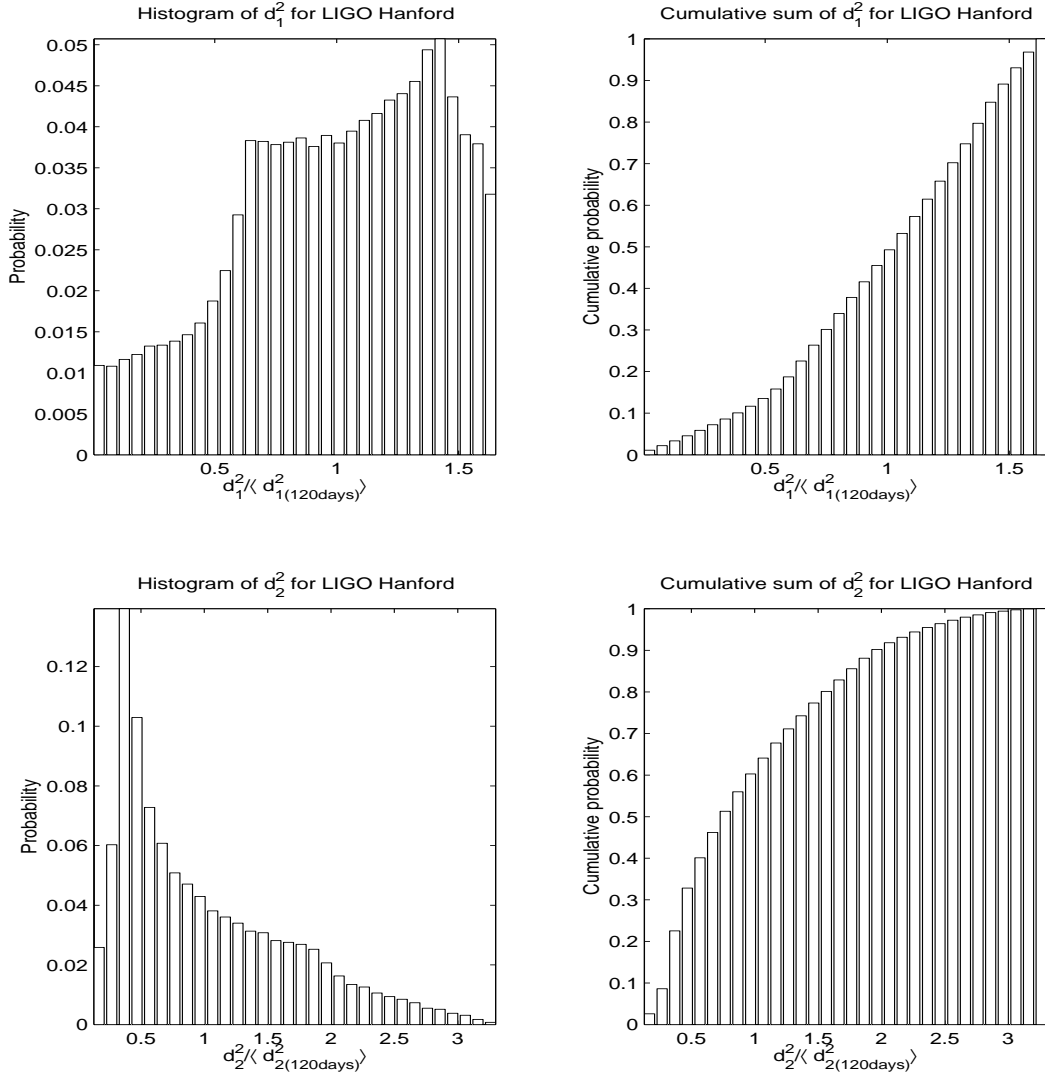
Figure 10: Histograms of the simulated probability density and cumulative distribution functions of the normalized signal-to-noise ratios $d_1^2/\langle d_{1(120\text{days})}^2\rangle$ and $d_2^2/\langle d_{2(120\text{days})}^2\rangle$ for the LIGO Hanford detector.
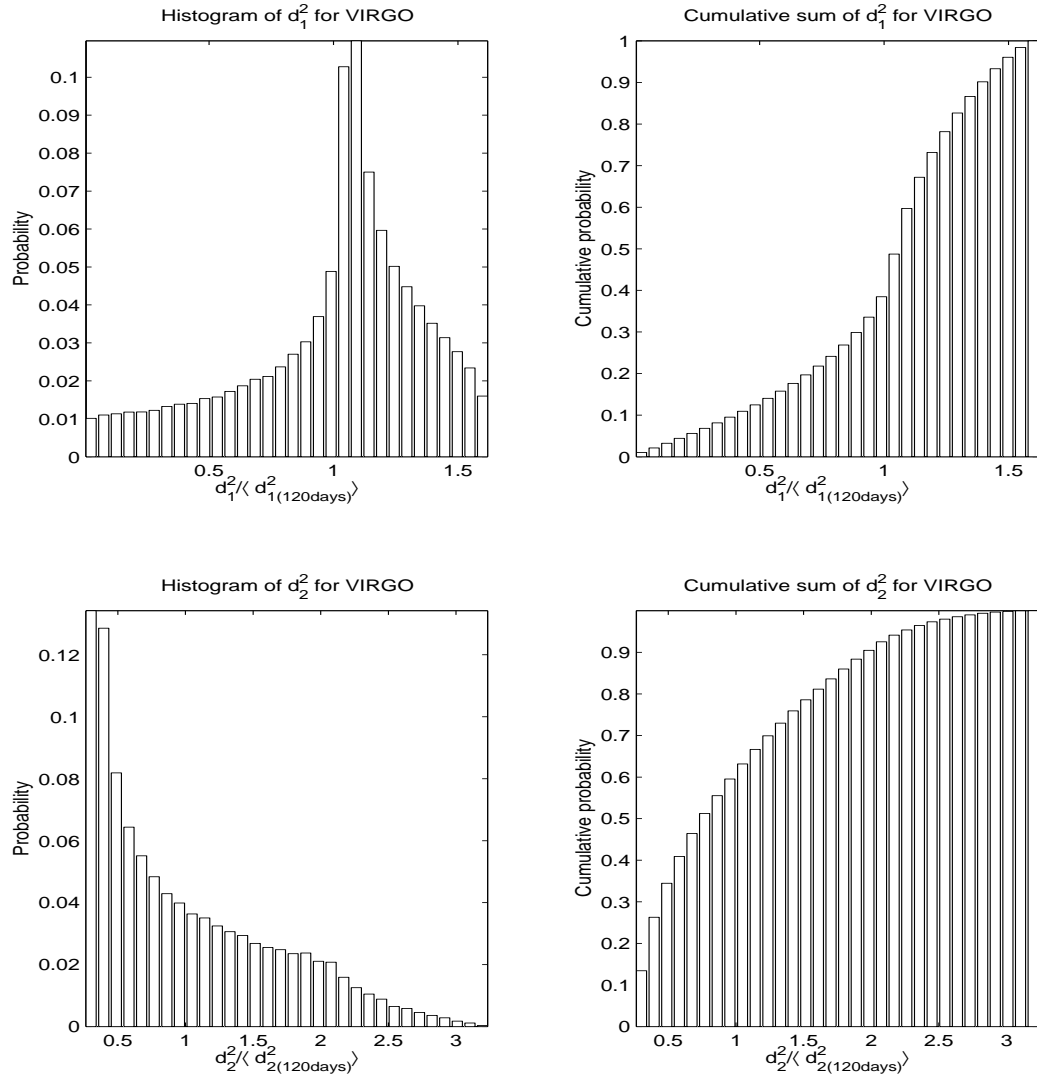
Figure 11: Histograms of the simulated probability density and cumulative distribution functions of the normalized signal-to-noise ratios $d_1^2/\langle d_{1(120\text{days})}^2 \rangle$ and $d_2^2/\langle d_{2(120\text{days})}^2 \rangle$ for the LIGO Livingston detector.

Figure 12: Histograms of the simulated probability density and cumulative distribution functions of the normalized signal-to-noise ratios $d_1^2/\langle d_{1(120\text{days})}^2 \rangle$ and $d_2^2/\langle d_{2(120\text{days})}^2 \rangle$ for the VIRGO detector.
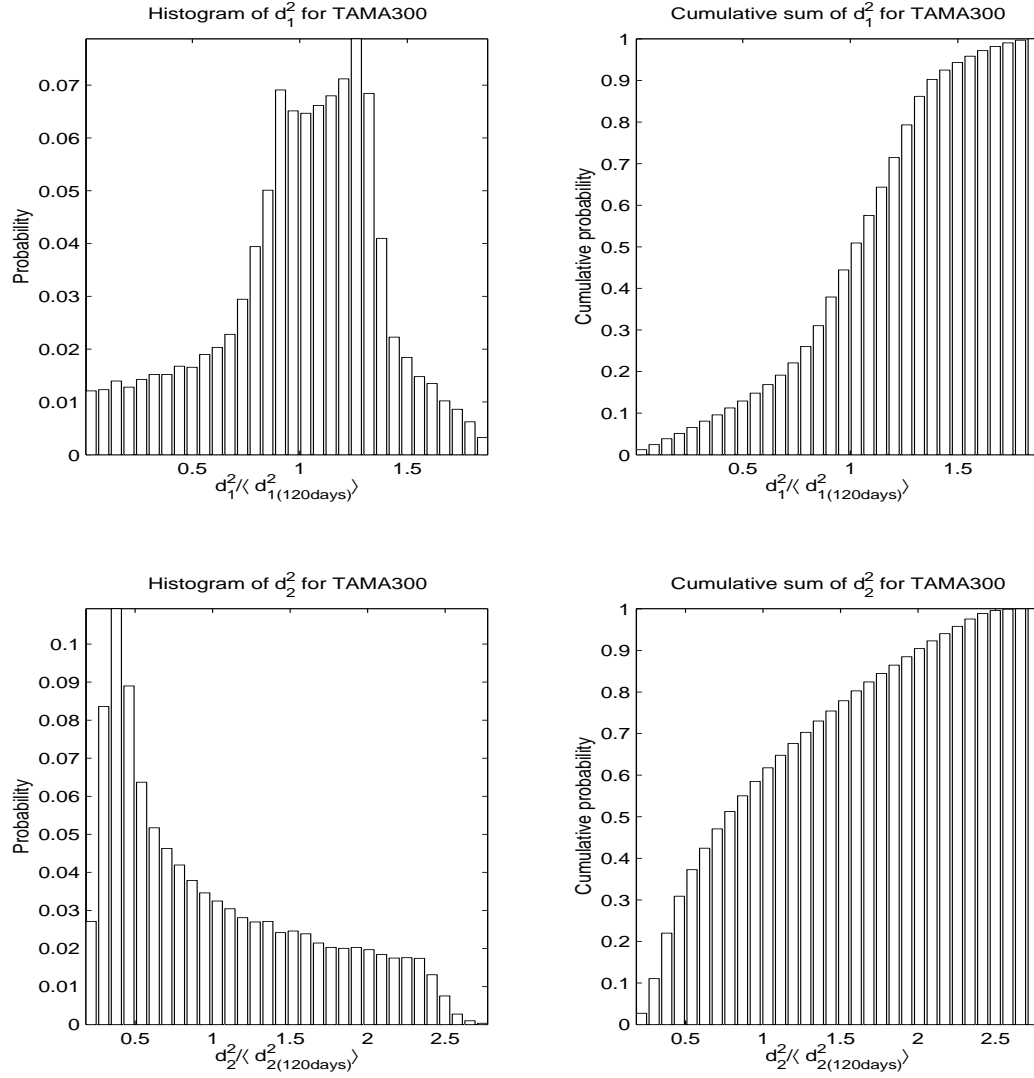
Figure 13: Histograms of the simulated probability density and cumulative distribution functions of the normalized signal-to-noise ratios $d_1^2/\langle d_{1(120\text{days})}^2 \rangle$ and $d_2^2/\langle d_{2(120\text{days})}^2 \rangle$ for the TAMA300 detector.